

COMPUTATIONAL GEOMECHANICS

Boris Jeremić

*Department of Civil and Environmental Engineering,
University of California,
Davis, CA, U.S.A.*

Kallol Sett

*Department of Civil Engineering,
University of Akron,
Akron, OH, U.S.A.*

Mahdi Taiebat

*Department of Civil Engineering,
University of British Columbia,
Vancouver, BC, Canada*

Nima Tafazzoli

*Department of Civil and Environmental Engineering,
University of California,
Davis, CA, U.S.A.*

version: 25. February, 2013, 16:43

Geomechanics, Modeling and Simulation, Elasto–plasticity, Statics and Dynamics.

Contents

Keywords:	1
1 Introduction	3
2 Theoretical and Computational Formulation	4
2.1 Finite Element Formulation	5
Deterministic Approach	5
Stochastic Approach	5
2.2 Elasto-Plasticity	5
Deterministic Elasto-Plasticity	5
Explicit and Implicit Algorithms	6
Probabilistic Elasto-Plasticity	7
2.3 Verification and Validation	8
Prediction	8
2.4 Software and Hardware Platform	9
3 Application to Practical Engineering Problems	10
3.1 Dynamics of Earthquake-Soil-Structure Systems	10
Staged Simulations	10
Soil Self-Weight Stage.	11
Piles, Columns and Superstructure Self-Weight Stage.	11
Seismic Shaking Stage.	11
Free Field vs. SSI Motions.	11
Bending Moments Response.	12
3.2 Dynamics of Saturated Soils	13
Isolation of Ground Motions in Level Ground	14
3.3 Probabilistic Geomaterial Response	17
Quantification of Uncertainties in Input Soil Parameters	17
Simulation of G/G_{max} and Damping Behavior	20
Probabilistic elastic-plastic stress-strain response.	20
Evolution of secant shear modulus.	21
4 Summary	23

1 Introduction

Computational geomechanics is a discipline of computational mechanics that models and simulates static and dynamic behavior of structures and solids made of geomaterials. Geomaterial is any pressure dependent, dilative/compressive, porous material, and it consists of porous matrix/skeleton and fluid in pores.

Pores of geomaterial can be filled with various fluids, most commonly with air (dry geomaterial), water (fully saturated geomaterial), oil (in petroleum engineering) or with mixtures of fluids (for example air and water, for partially saturated geomaterial). Porous matrix/skeleton of geomaterial is usually modeled as continuum material, using incremental theory of elasto–plasticity and a number of elastic–plastic material models of various complexity.

Mechanical behavior of geomaterials is intrinsically connected to the full interaction, coupling between porous matrix/skeleton and the pore fluid. Full coupling is modeled through the application of effective stress principle. The effective stress is defined as $\sigma'_{ij} = \sigma_{ij} + \delta_{ij}p$ where σ_{ij} is total stress, δ_{ij} is Kronecker delta, and p is the pore fluid pressures. It is important to note that stress is defined positive in tension, while pore fluid pressure is positive in compression. In some cases, when only air is present in pores and coupling effects of pore fluid (air) and porous skeleton can be neglected, modeling and simulation can be done for single phase, dry geomaterial.

Two main approaches to modeling solids and structures made of geomaterials are therefore possible. In a single phase approach, neglected is the pore fluid (usually air) and simulations are done using total stresses. On the other hand, two phase modeling and simulations are used when coupling and influence of pore fluid on porous skeleton (and vice versa) cannot be neglected. Two phase modeling and simulation is more general and can be used for single phase problems as well. It is noted that there are problems where more than two phases (porous solid and pore fluid) are contributing to the behavior of solids and structures made of geomaterials. For example, in addition to single fluid (water or air for example) there are problems where two (water and air) or three (water, air and oil) fluid phases affect geomaterial response. In addition to behavior of porous skeleton and pore fluid, other fields can have important interactions/influences and affect behavior of geomaterials. Mentioned are temperature and electrical fields that in some cases need to be properly modeled and simulated for proper prediction of behavior of geomaterials.

In this overview chapter, only single and two phase modeling and simulation approaches will be covered (in sections

Computational Geomechanics uses computational models to simulate the state of a geomechanics system upon application of generalized loads. Computational simulations can in general be used for verification, validation and predictions. Confidence in predictions relies heavily on proper verification and validation process. Verification is the process of determining that a model implementation accurately represents the developer's conceptual description and specification. It is a mathematics issue and it provides evidence

that the model is solved correctly. Validation is the process of determining the degree to which a model is accurate representation of the real world from the perspective of the intended uses of the model. It is a physics issue and it provides evidence that the correct model is solved. Computational Prediction is the process of foretelling the state of a geomechanics system under conditions for which the computational model has not been validated. Verification and Validation procedures are the primary means of assessing accuracy in modeling and computational simulations and are essential tools in building confidence and credibility in computational Predictions.

2 Theoretical and Computational Formulation

Computational formulation for geomaterials is most commonly based on incremental theory of elasto-plasticity and static equilibrium, for static problems, and dynamic equations of motions, for dynamic problems.

Consider the dynamic equilibrium (equation of motion) for a general three-dimensional solid made of any (geo-)material. The external forces (surface tractions, body and inertial forces) are in equilibrium with internal and inertial forces. The weak form of dynamic equilibrium equation for such a solid, assuming general, large deformations, can be written as¹.

$$\int_{V_0} \delta u_{i,j} P_{ij} dV = \int_{V_0} \rho_0 \delta u_i b_i dV - \int_{S_0} \delta u_i \bar{t}_i dS \quad (1)$$

where u_i are (generalized) displacements (and $u_{i,j} = \partial u_i / \partial x_j$), P_{iJ} is the first Piola-Kirchhoff stress tensor, ρ_0 is the initial material density, b_i are body (including inertial) forces and \bar{t}_i surface tractions. It is important to note that general, large deformations are assumed, using Lagrangian strain tensor $E_{IJ} = \frac{1}{2} (u_{I,J} + u_{J,I} + u_{K,I} u_{K,J})$ While it is very appropriate to perform the analysis using real deformations, most of the time it proves beneficial to make simplifying assumption of small deformation, in which case the last term in the above equation is neglected, yielding a small deformation strain $\epsilon_{ij} = \frac{1}{2} (u_{i,j} + u_{j,i})$. With the assumption of small deformations, first Piola-Kirchhoff stress P_{ij} can be replaced with Cauchy stress σ_{ij} . The above equation can be solved to determine displacements of a soil or structure loaded with general, time varying forces.

¹Assuming index summation rule .

2.1 Finite Element Formulation

Deterministic Approach Upon discretization into finite elements, and after some algebraic manipulations, the discretized system of equations can be written as

$$M_{PQ} \ddot{u}_P + K_{PQ} \bar{u}_P = F_Q \quad P, Q = 1, 2, \dots, (DOF \text{ per Node})N \quad (2)$$

where M_{PQ} is system mass matrix, K_{PQ} is system stiffness matrix and F_Q is the loading vector, while \ddot{u}_P and \bar{u}_P are nodal accelerations and displacements respectively. It is important to note that damping terms, representing velocity proportional energy dissipation, results from coupling of solid and fluid phases of analyzed domain, or can be approximated by Rayleigh and Cauchy damping. In addition to velocity proportional, displacement proportional damping plays a major role in energy dissipation phenomena and is introduced by elastic-plastic yielding of materials, introduced in a section 2.2.

Stochastic Approach Behavior of realistic solids and structures is in essence uncertain, stemming from uncertain material behavior and uncertain loading. A simplification of probabilistic, realistic modeling is the deterministic approach described briefly above. One of the more prominent approaches to modeling stochastic (uncertain) behavior of elastic solids and structures is based on the Spectral Stochastic Finite Element Method, while the probabilistic elastic problems are modeled using Stochastic Elastic-Plastic Finite Element method.

2.2 Elasto-Plasticity

One of most prominent approaches to modeling material nonlinear response of solids and structures is based on the incremental theory of elasto-plasticity. In general, large deformations modeling is needed, with a commonly used multiplicative decomposition of the deformation gradient into elastic and plastic parts $F_{ij} \stackrel{\text{def}}{=} F_{ki}^e F_{kj}^p$ where the deformation gradient is defined as $F_{kK} = x_{k,K}$. For isotropic and monotonic loading problems, where principal directions of stress and strain remain colinear during loading, spectral decomposition family of algorithms is applicable, while for general anisotropic and/or cyclic problems a Taylor's series expansion family of algorithms must be used.

Focus will be shifted to small deformation problems where multiplicative decomposition of the deformation gradient can be approximated by the additive decomposition of strain into elastic and plastic components. Some details are provided below.

Deterministic Elasto-Plasticity A wide range of elasto-plastic materials can be characterized by means of a set of constitutive relations of the general form:

$$d\epsilon_{ij} = d\epsilon_{ij}^e + d\epsilon_{ij}^p \quad (3)$$

$$d\sigma_{ij} = E_{ijkl} d\epsilon_{kl}^e \quad (4)$$

$$d\epsilon_{ij}^p = d\lambda \frac{\partial Q}{\partial \sigma_{ij}} = d\lambda m_{ij}(\sigma_{ij}, q_*) \quad (5)$$

$$dq_* = d\lambda h_*(\tau_{ij}, q_*) \quad (6)$$

where, following standard notation ϵ_{ij} , ϵ_{ij}^e and ϵ_{ij}^p denotes the total, elastic and plastic strain tensor, σ_{ij} is the Cauchy stress tensor, and q_* signifies some suitable set of internal variables². The asterisk in the place of indices in q_* replaces n indices³. Equation (3) expresses the commonly assumed additive decomposition of the infinitesimal strain tensor into elastic and plastic parts. Equation (4) represents the generalized Hooke's law which linearly relates stresses and elastic strains through a stiffness modulus tensor E_{ijkl} . Equation (5) expresses a generally associated or non-associated flow rule for the plastic strain and (6) describes a suitable set of hardening laws, which govern the evolution of the plastic variables. In these equations, m_{ij} is the plastic flow direction, h_* the plastic moduli and $d\lambda$ is a plastic parameter to be determined with the aid of the loading—unloading criterion, which can be expressed in terms of the Karush–Kuhn–Tucker condition as:

$$F(\sigma_{ij}, q_*) \leq 0 \quad ; \quad d\lambda \geq 0 \quad ; \quad F d\lambda = 0 \quad (7)$$

Explicit and Implicit Algorithms Elastic-Plastic differential equation are most commonly solved using either explicit (aka forward Euler) or implicit (aka backward Euler) algorithms. It is noted that there exists a range of generalized mid point integration algorithms, however they are rarely used for practical computations.

The explicit algorithm (Forward Euler) is based on using the starting point (the state stress σ_{ij}^n and internal variable space q_*^n on the yield surface) for finding all the relevant derivatives and variables. After some tensor algebra and manipulations, the increments in stress tensor and internal variables can be written as

$$d\sigma_{mn} = E_{mnpq} d\epsilon_{pq} - E_{mnpq} \frac{{}^n n_{rs} E_{rstu} d\epsilon_{tu}}{{}^n n_{ab} E_{abcd} {}^n m_{cd} - \xi_A h_A} {}^n m_{pq} \quad (8)$$

$$dq_A = \left(\frac{{}^n n_{mn} E_{mnpq} d\epsilon_{pq}}{{}^{cros} n_{mn} E_{mnpq} {}^{cros} m_{pq} - \xi_A h_A} \right) h_A \quad (9)$$

where ${}^n()$ denotes the starting elastic–plastic point for that increment. It should be noted that the explicit algorithm performs only one step of the computation and does not check on the equilibrium of the obtained solutions. This usually results in the slow drift of the stress-internal variable point from the yield surface for monotonic loading. It also results in spurious plastic deformations during elastic unloading for cyclic loading-unloading.

²In the simplest models of plasticity the internal variables are taken as either plastic strain components ϵ_{ij}^p or the hardening variables κ defined, for example as a function of inelastic (plastic) work, i.e. $\kappa = f(W^p)$. See page 115.

³for example ${}_{ij}$ if the variable is ϵ_{ij}^p , or nothing if the variable is a scalar value, i.e. κ .

The continuum tangent stiffness tensor (${}^{cont}E_{pqmn}^{ep}$) that is obtained for the explicit integration procedure has the following form:

$${}^{cont}E_{pqmn}^{ep} = E_{pqmn} - \frac{E_{pqkl} n_{mkl} n_{ij} E_{ijmn}}{n_{ot} E_{otrs} n_{mrs} - n_{\zeta A} h_A} \quad (10)$$

It is important to note that continuum tangent stiffness (${}^{cont}E_{pqmn}^{ep}$) posses minor symmetries (${}^{cont}E_{pqmn}^{ep} = {}^{cont}E_{qpnm}^{ep} = {}^{cont}E_{pqnm}^{ep}$), while major symmetry (${}^{cont}E_{pqmn}^{ep} = {}^{cont}E_{mnpq}^{ep}$), is only retained for associated elastic–plastic materials, when $n_{ij} \equiv m_{ij}$.

Implicit (backward Euler) algorithm, described briefly below, has the advantage of implicitly using the plastic flow return at the final solution point in stress and internal variable space. Finding the final solution point requires iterations, which adds to complexity and computational load. However, iterations allow for equilibrium tolerance to be prescribed (small as required) and enforced during iterations. Formulation and iterative procedure for the backward Euler constitutive integration are given in books and will not be repeated here due to space constraints.

Probabilistic Elasto-Plasticity While elastic-plastic constitutive theory is fairly well developed, with appropriate models for various geologic materials, when material parameters are treated as deterministic, spacial variability and material behavior uncertainty have not been treated in any depth. Recent development of Probabilistic Elasto-Plasticity (PEP) and Stochastic Elastic-Plastic Finite Element Method (SEPFEM) allows for accurate solution of elastic–plastic problems with fully probabilistic material parameters that are spatially variable. Solution to the PEP problem is based on the extension of constitutive rate Eq. (8) into probability density space using Eulerian–Lagrangian Fokker–Planck–Kolmogorov approach. Resulting advection diffusion equation

$$\frac{\partial P(\sigma_{ij}, t)}{\partial t} = -\frac{\partial}{\partial \sigma_{ab}} \left[N_{ab}^{(1)} P(\sigma_{ij}, t) - \frac{\partial}{\partial \sigma_{cd}} \left\{ N_{abcd}^{(2)} P(\sigma_{ij}, t) \right\} \right]$$

can be solved for the probability density of stress tensor $P(\sigma_{ij}, t)$. Approach is applicable to any incremental elastic–plastic model, and only coefficients $N_{ab}^{(1)}$ and $N_{abcd}^{(2)}$ need to be derived for different material models. Solution provides a complete probabilistic description of response, and is second-order exact to covariance of time (exact mean and variance).

While the above PEP approach takes into account point wise uncertain behavior, spatial variability is modeled using SEPFEM. To this end, uncertain spatial variability of soil properties, generally modeled as random fields, is discretized into random variables using Karhunen–Loève expansion. Those random variables are then propagated through the PEP and spatial average constitutive response is assembled using a stochastic finite element technique. Polynomial chaos expansion and Galerkin technique, are used to form SEPFEM equations that are solved to obtain full probabilistic response for all degrees of freedom.

2.3 Verification and Validation

Developing a strong assurance of accurate numerical predictions of the seismic response of Nuclear Power Plant Soil Structure System (NPPSSS) rely heavily on **Verification and Validation** (V&V) procedures. Verification and validation procedures are the primary means of assessing accuracy in modeling and computational simulations. Verification is the process of determining that a model implementation accurately represents the developer's conceptual description and specification. Verification provides evidence that the model is solved correctly. It is essentially a mathematics issue. Validation is the process of determining the degree to which a model is an accurate representation of the real world from the perspective of the intended uses of the model. Validation provides evidence that the correct model is solved. It is essentially a physics issue. V&V procedures are the tools with which we build confidence and credibility in numerical predictions resulting from modeling and computational simulations. Figure 1 shows role of verification and validation in modeling and simulating real world NPPSSSs.

Figure 1: Schematic representation of role of verification and validation in relation to real model

It is very important to note that a tight coupling exists between each of the phases of modeling and simulation process shown in Figure 1. Figure 2 shows a more detailed view of relationship of verification and validation to the developed computational solution.

Figure 2: Schematic representation of relationship between verification and validation

It is also important to note that verification procedures include software quality assurance practices, which are based on an extensive (fully and semi-) automatic test suite (eg. regression testing, white and gray box testing, static and dynamic testing, etc.).

The main motivation for performing verification stems from the simple question: "how much can you trust model implementations?". Validation, on the other hand can be motivated by the question: "how much can your trust numerical simulations?". Both questions can be summarized by the question: "how good are our numerical predictions in simulating real world NPPSSSs?". In relation to numerical prediction of seismic performance of NPPSSSs, the question can also be rephrased: "can numerical simulation tools (NRC ESSI Simulator for example) be used for assessing public safety?".

Prediction Numerical prediction comprises use of computational model to foretell the state of an object (NPPSSS in this case) under conditions for which the computational model has not been fully validated,

typically due to its complexity. It is important to note that validation does not directly make a claim about the accuracy of a prediction since computational models can be easily misused (unintentionally or intentionally). Accuracy of prediction is closely related to how closely related the conditions of the prediction and the specific cases in the validation database are; and how well is physics of the problem understood. Validation and application domains rarely have any significant overlap. Figure 3 shows two such cases, left side showing partial overlap and the right side showing complete lack of overlap.

Figure 3: Schematic representation of partial or no overlap of verification and application domains

For seismic behavior of NPPSSSs, partial overlap is potentially available for small seismic events (somewhat frequent) where the response of a complete NPPSSS can be recorded (depending on the extent of installed instrumentation). In this case, numerical predictions could be validated against such recordings. However, in the case of numerical simulations for predicting NPPSSS behavior during significant (rare, catastrophic) seismic events, overlap with validation cases is non-existent and application domain behavior has to be inferred through numerical simulations. Such inference needs to be based on rational mechanics of all important phenomena that affect NPPSSS behavior. It must also account for uncertain nature of material parameters, seismic loading and other components of NPPSSS. Ever present uncertainty needs to be properly estimated and modeled for numerical predictions. It is important to identify all sources of uncertainty, create mathematical representation of individual sources, and propagate those uncertainties through modeling and simulation process.

2.4 Software and Hardware Platform

Formulations and algorithms described in previous sections are organized in numerical libraries following the library centric design approach.

The finite element domain is managed using Modified OpenSees Services (MOSS) library . On a lower functional level, a set of Template3Dep and NewTemplate3Dep numerical libraries are used for constitutive level modeling, while nDarray numerical libraries are used to handle vector, matrix and tensor manipulations, and FEMtools element libraries from UCD CompGeoMech toolset are used to supply other necessary libraries and components. The solution of system of equations is provided by public domain solvers, PETSc, or UMFPACK. A parallel processing simulation model (desirable for full 3D NPPSSS modeling) is based on the Plastic Domain Decomposition (PDD) method , with graph partitioning based on ParMETIS libraries.

Numerical libraries organized in such way are then used to create application programs that are specifically tailored for particular application problems. One such application program is the NRC ESSI Simulator

Program, developed for dynamic/seismic analysis of Nuclear Power Plants under full 3D, inclined, incoherent seismic motions including body and surface waves.

3 Application to Practical Engineering Problems

In this section, examples will be used to illustrate application of computational geomechanics tools to practical problems. Three such practical problems will be addressed. First example deals with the interaction of earthquake with the soil-structure system (in section 3.1). Second examples investigates the behavior of fully saturated soil under dynamic loading (in section 3.2), while the third example, in section 3.3, presents results from a probabilistic elastic-plastic modeling in geomechanics.

3.1 Dynamics of Earthquake-Soil-Structure Systems

The dynamic interaction of earthquake, soil and structure represents the most significant seismic effect. Such interaction can be beneficial or detrimental to the dynamic behavior of the soil-structure system.

As an example, a bridge soil-structure system, model of which is shown in Figure 4 was analyzed for a two different soil conditions and for two different earthquakes. First model features soft soil (representing soft mud, underlaid by dense sand) while second model featured stiff soil (dense sand). Both models were used for seismic analysis of a soil bridge system under Northridge (predominant high frequency) and Kocaeli (predominant low frequency) earthquakes. The bridge structure (foundation piles, piers and superstructure) were the same in both soft and stiff soil models.

Figure 4: Detailed Three Bent Prototype SFSI Finite Element Model, 484,104 DOFs, 151,264 Elements used for most simulation in this study

The finite element model(s) used in this study have combined both elastic-plastic solid elements, used for soils, and elastic and elastic-plastic structural elements, used for concrete piles, piers, beams and superstructure. Of particular importance for accurate modeling was the size of soil element, which if chosen to large will (artificially) filter seismic waves of certain frequencies. Such element size requirement created a need for very large meshes, largest of which had over half a million elements and over 1.5 million degrees of freedom. Seismic ground motions were applied to the SSI finite element model using the Domain Reduction Method (DRM).

Staged Simulations Application of loads in stages is essential for nonlinear, elastic-plastic models. This is especially true when modeling soil and concrete. Staged loading ensures appropriate initial conditions

for each loading stage. Modeling starts from a zero stress and deformation state, on level ground, with no foundations or bridge structure. Three loading stages, described below, then follow.

Soil Self-Weight Stage. During this stage the finite element model for soil (no structure) is loaded with soil self-weight. The finite element model for this stage excludes any structural elements, the opening (hole) where the pile will be placed is full of soil. Displacement boundary conditions on the sides of the three soil blocks are such that they allow vertical movements, and allow horizontal in boundary plane movement, while they prohibit out of boundary plane movement of soils. All the displacements are suppressed at the bottom of all three soil blocks. The soil self weight is applied in 10 incremental steps.

Piles, Columns and Superstructure Self-Weight Stage. In this, second stage, number of changes to the model happen. First, soil elements where piles will be placed are removed (excavated), then concrete piles (beam-column elements) are placed in the holes (while appropriately connecting structural and solids degrees of freedom), columns are placed on top of piles and finally the superstructure is placed on top of columns. All of this construction is done at once. With all the components in place, the self weight analysis of the piles-columns-superstructure system is performed.

Seismic Shaking Stage. The last stage in our analysis consists of applying seismic shaking, by means of effective forces using DRM. It is important to note that seismic shaking is applied to the already deformed model, with all the stresses, internal variables and deformation that resulted from first two stages of loading.

Bridge model described above was used to analyze a number of cases of different foundation soils and earthquake excitations. Two sets of ground motions were used for the same bridge structure. Variation of foundation soil, namely (a) all stiff sand and (b) all soft clay. Ground motions for Northridge and Kocaeli earthquakes (free field measurement, see Figure 5) were used in determining appropriate wave field (using DRM). Since the main aim of the exercise was to investigate SFS system a set of short period motions were chosen among Northridge motions records, while long period motions from Kocaeli earthquakes were used for long period example.

Figure 5: Input motions: short period (Northridge) and long period (Kocaeli)

A number of very interesting results were obtained and are discussed below.

Free Field vs. SSI Motions. A very important aspect of SFSI is the difference between free field motions and the motions that are changed (affected) but the presence of the structure. Figure 6 shows comparison of

free field short period motions (obtained by vertical propagation of earthquake motions through the model without the presence of bridge structure and piles) and the ones recorded at the base of column of the left bent in stiff and soft soils.

Figure 6: Comparison of free field versus measured (prototype model) motions at the base of left bent for the short period motions (Northridge) for all clay (CCC) and all sand (SSS) soils

It is immediately obvious that the free field motions in this case do not correspond to motions observed in bridge SFS system with stiff or soft soils. In fact, both the amplitude and period are significantly altered for both soft and stiff soil and the bridge structure. This quite different behavior can be explained by taking into account the fact that the short period motions excite natural periods of stiff soil and can produce (significant) amplifications. In addition to that, for soft soils, significant elongation of period is observed.

On the other hand, as shown in Figure 7, the same SFS system (same structure with stiff or soft soil beneath) responds quite a bit different to long period motions.

Figure 7: Comparison of free field versus measured (prototype model) motions at the base of left bent for the long period motions (Kocaeli) for all clay (CCC) and all sand (SSS) soils

The difference between free field motions and the motions measured (simulated) in stiff soils is smaller in this case. This is understandable as the stiff soil virtually gets carried away as (almost) rigid block on such long period motions. For the soft soil one of the predominant natural periods of the SFS system is excited briefly (at 12-17 seconds) but other than that excursion, both stiff and soft soil show fair matching with free field motions. In this case the SFS effects are not that pronounced, except during the above mentioned period between 12 and 17 seconds.

Bending Moments Response. Influence of variable soil conditions and of dynamic characteristic of earthquake motions on structural response is followed by observing bending moment response. For this particular purpose, a time history of bending moment at the top of one of the piers of bent # 1 (left most in Figure 4) is chosen to illustrate differences in behavior.

Figure 8 shows time history of the bending moment at top of left most pier of bent # 1 for all sand (SSS) and all clay (CCC) cases for short period motion (Northridge).

Figure 8: Simulated bending moment time series (top of left pier) for short period motion (Northridge), for all clay (CCC) and all sand (SSS) soils

Similarly, Figure 9 shows time history of the bending moment for same pier, for same soil conditions, but for long period motion (Kocaeli).

Figure 9: Simulated bending moment time series (top of left pier) for long period motion (Kocaeli), for all clay (CCC) and all sand (SSS) soils

Time histories of bending moments are quite different for both types of soil conditions (SSS and CCC) and for two earthquake motions. For example, it can be seen from Figure 8 that short period motion earthquake, in stiff soil (SSS) produces (much) larger plastic deformation, which can be observed by noting flat plateaus on moment – time diagrams, representing plastic hinge development. Those plastic hinge development regions are developing symmetrically, meaning that both sides of the pier have yielded and full plastic hinge has formed. On the other hand, the short period earthquake in soft soil (CCC) produces very little damage, one side of a plastic hinge is (might be) forming between 14 and 15 seconds.

Contrasting those observation is time history of bending moments in Figure 9, where, for a long period motion, stiff soil (SSS) induces small amount of plastic yielding (hinges) on top of piers. However, soft soil (CCC) induces a (very) large plastic deformations. Development of plastic hinges for a structure in soft soil also last very long (more than two seconds, see lower plateau for CCC case in Figure 9) resulting in significant damage development in thus formed plastic hinges. Observed behavior also somewhat contradicts common assumption that soft soils are much more detrimental to structural behavior. It is actually the interaction of the dynamic characteristic of earthquake, soil and structure (ESS) that seem to control the ultimate structural response and the potential damage that might develop.

3.2 Dynamics of Saturated Soils

Liquefaction of level and sloping ground represents a common situation during earthquakes. It is therefore of interest to use the developed numerical tool for simulating the earthquake wave propagation in such cases.

This section presents results of numerical simulation for different cases of a 1D site response, using the available 3D elements in the developed numerical simulation tool. Two general examples have been studied. The first example presents results of a study on the isolating effect of a liquefied sand layer in propagation of seismic waves. In the second example the seismic induced shear deformation of a gentle slope in presence or absence of liquefiable layer has been studied.

It should be noted that the simulations are based on the small deformation assumption, which might introduce large error in strain tensor (by neglecting quadratic portion of displacement derivatives) when soil undergoes large deformations.

Isolation of Ground Motions in Level Ground A 10m vertical column of saturated sand consisting of twenty $u - p - U$ eight-node brick elements was considered subjected to an earthquake shaking at the base. Two particular cases have been studied in this example. In the first case, all 20 elements of the soil column are assumed to be at medium dense state at the beginning of analysis ($e_{in} = 0.80$). In the second case, the deepest two meters of the soil column are assumed to be at looser initial states compared to the first case. In particular two of the deepest elements are assumed to be at $e_{in} = 0.95$ (loose) and the next two elements at $e_{in} = 0.875$ (medium loose), just to make a smoother transition between the loose and dense elements. The rest of the soil column, i.e. the upper 16 elements (8 meters) are at the same density as the first case ($e = 0.80$). A schematic illustration of these two cases is presented in Figure 10.

Figure 10: Illustration of the problem in terms of the soil layering, the finite element mesh, and the input base acceleration

The elements are labeled from E01 (bottom) to E20 (surface) in Figure 10. The boundary conditions are such that the vertical displacement degrees of freedom (DOF) of the soil and water at the base ($z = 0$) are fixed, while the pore pressure DOFs are free. The soil and water vertical displacement DOFs at the surface ($z = 10m$) are free to simulate the upward drainage. The pore pressure DOFs are fixed at the surface. On the sides, soil skeleton and water are prevented from moving in the y direction while movements in x and z directions are free. It is emphasized that the displacements of soil skeleton and pore fluid are different. In order to simulate the 1D behavior, all of the related DOFs of the nodes at each depth are connected in a master–slave fashion, i.e. the nodes at the same level have the same u_i ($i=x,y,z$). Same thing is true for p and U_i . The values of u_i and U_i however may be different at a node, allowing for relative movement of soil and fluid. The soil is assumed to be Toyoura sand and is characterized by the validated SANISAND model . The permeability is assumed to be isotropic and equal to $k = 5.0 \times 10^{-4}$ m/s.

A self-weight analysis was performed before the base excitation. The resulting fluid hydrostatic pressures and soil stress states along the soil column serve as initial conditions for the subsequent dynamic analysis. An input acceleration time history (Figure 10), taken from the recorded horizontal acceleration of Model No.1 of VELACS project at RPI , was considered in which $a_{max} = 0.2g$ and main shaking lasts for about 12 seconds.

In addition to the [physical] velocity and displacement proportional damping from the element and the material model, respectively, a small amount of numerical damping has been introduced through constants of the HHT algorithm in order to stabilize the dynamic time stepping. No Rayleigh damping has been used.

Results of the analysis during and after the shaking phase for both cases (i.e. the uniform and the layered soil profiles) are presented in Figures 11 and 12.

Figure 11: (left) Variation of shear stress σ_{xz} vs vertical effective stress σ_z for Elements E01 – E19 during and after shaking; (right) Variation of shear stress σ_{xz} vs shear strain γ for Elements E01 – E19 during and after shaking

Figure 12: (left) Variation with time of void ratio e for Elements E01 – E19 during and after shaking ; (right) Time history of horizontal component of acceleration in solid part of the mixture $a_{u,x}$ for nodes at different elevations during shaking

In all these figures the plots on the left and right correspond to the cases of uniform and layered soil profiles, respectively. In particular, Figure 11 show variations of the shear stress σ_{xz} vs vertical effective stress σ_z and shear strain γ , respectively. Figure 12 show time histories of void ratio e (left) and horizontal (x) component of acceleration in solid part of the mixture $a_{u,x}$ (right), respectively. Note that different rows of plots in Figures 11 and 12 correspond to different elements. Similarly, different rows in Figure 12(right) correspond to different elevations of the nodes.

Figure 11a shows the typical mechanism of cyclic decrease in vertical effective stress for the case of the uniform soil column. Signs of the so-called butterfly loops in the effective stress path can be observed partially from early stages of shaking at the upper layer as these layers are in lower confining pressures compared to the deeper layers and thus are more dense than critical in the critical state soil mechanics terminology, i.e. with less contractive tendency. In later stages of shaking, when the confining pressures are reduced to smaller values, the butterfly shapes of the stress paths are more pronounced and almost all depths of the soil column experience the cyclic mobility mechanism of liquefaction. In this stage the soil layers momentarily experience small values of effective stress followed by a dilative response in which the elements recover their strength in cycles of loading due to their denser than critical state. As a result, the seismic-induced shear waves propagate all the way to the surface of the soil column. The response can be observed as an average degradation of stiffness and accumulation of shear strains in all levels of the soil column as shown in Figure 11(right).

In case of the layered soil profile, however, Figure 11b shows that the first cycle of shaking degrades the vertical effective stress in the loose layer of element 1, E01, to very small values in a flow liquefaction mechanism. The shear wave in this first cycle of shaking propagates to the surface and causes some reduction in vertical effective stress in upper soil layers. Because element 1, E01, is in loose states and has a strong contractive tendency it does not recover its strength in cyclic loading and therefore it remains in this liquefied state after the first cycle with negligible shear resistance. Therefore this layer acts as an isolating layer and no shear stress can be transmitted to the upper layers after the first cycle. This mechanism can also be observed in the shear stress – shear strain plot of Figure 11(right) as the first cycle completely liquefies the E01 and

after this cycle no shear stress is propagated to the upper layers. Of course the very loose element E01 shows considerable amount of shear strain due to liquefaction. As it is shown in Figure 11b in upper layers after the first cycle of shaking no reduction in vertical effective stress occurs due to shearing (induced by shaking) in these layers, however, one can observe that the vertical effective stress keeps decreasing in upper layers during (and even for a while after) shaking. This is because the dissipated pore pressure in deeper layers travels upward and reduces the effective stress in upper layers. The effective stress will then start to recover as the excess pore pressure dissipates from these layers.

Figure 12 shows the redistribution of void ratio during and long after the shaking. The horizontal dashed line in each plot shows $e_{in,shaking}$ that is the value of void ratio for the corresponding layer at the beginning of shaking (at the end of self-weight analysis). For the uniform soil column Figure 12a shows a general trend of consolidation in all of the soil layers. This consolidation starts later in upper layers because of the water pumped from the lower layers, which is to be dissipated by time. In the layered soil column (Figure 12b) the loose layer in element 1, E01, shows considerable consolidation due to shaking. The dissipated volume of water from this layer is pumped to the upper layers and result is some dilation (increase in void ratio) in the these layers for some time after the end of shaking. By the time this pumped volume of water in the upper layers dissipates all the layers show a consolidation response. In other words in the layered soil column pumping of water causes initial loosening of soil in the upper layers, which is then followed by densification.

Finally Figure 12(right) shows propagation of the horizontal acceleration through the soil column during shaking. In the uniform soil column First of Figures 12(right) shows that the base acceleration is transmitted to the surface of the soil column. It shows some spikes of acceleration with large amplitude at the surface of the soil resulting from the dilative phases of soil response during the shaking phase. In the layered soil column, however, Second Figure 12(right) shows that only the first cycle of shaking is transmitted to the surface (although with reduced amplitude) and subsequently the upper layers are isolated because of the fully liquefied state of the loose layer in element 1, E01. The transmitted accelerations to the surface of the soil column after the first cycle of shaking have very small amplitudes.

3.3 Probabilistic Geomaterial Response

In this section, the constitutive behavior of normally consolidated, high plasticity clay is simulated probabilistically using the FPKE approach described in the previous section. Elastic–perfectly plastic von Mises material model is used for clay. The model requires shear modulus (G_{max}) and the undrained shear strength (s_u) as input soil parameters. Both the soil parameters are easily obtainable through transformation from commonly used in-situ measured properties, for example SPT N -value⁴, used in this paper.

Quantification of Uncertainties in Input Soil Parameters Transformation from measured in-situ properties to mechanical properties usually introduces uncertainty, which is currently (in traditional deterministic analysis) accounted for by applying engineering judgment. Alternatively, under the framework of probability theory, one could quantify the transformation uncertainty by modeling it as a random variable. For example, for alluvial clays in Japan, proposed the following relationship between SPT N -value and undrained shear strength (s_u):

$$s_u = 0.29 p_a N^{0.72} \quad (11)$$

where $p_a = 101,325\text{Pa}$ is the atmospheric pressure. The above relationship (Eq. (11)), along with the data from which the relationship is developed, is plotted in Figure 13.

Figure 13: Transformation relationship between SPT N -value and undrained shear strength, s_u

The data-scatter in Figure 13 represents knowledge uncertainty in the above transformation equation (Eq. (11)), and under probability theory, can be modeled as a random variable. To this end, Eq. (11), can be written as:

$$s_u = 0.29 p_a N^{0.72} + \chi \quad (12)$$

where, χ is a zero-mean random variable and represent the data-residual with respect to the deterministic transformation equation. The histogram of the residual is plotted in Figure 14. Regarding the model for the best-fit probability density function, a Normal distribution can be ruled out as the histogram is skewed. After trying few distributions, a Pearson IV type distribution, with Pearson parameters of 0, 2400, -2.75×10^5 , and 9×10^8 , was found to best fit the residual. The fitted pdf is shown in Figure 14.

Figure 14: Histogram of the residual (w.r.t the deterministic transformation equation) undrained strength, along with fitted probability density function

⁴We understand the limitations of using SPT N -value for the (deterministic) estimation of s_u and G_{max} for clay. However, our intent is to demonstrate the power of a simple constitutive model, that is extended into probabilistic space (stochastic material parameters), to simulate the actual response of soil

Similarly, for transformation between SPT N -value and Young's modulus (E) for alluvial clays in Japan, proposed a transformation equation, which can be written in probabilistic form as

$$E = 19.3 p_a N^{0.63} + \chi \quad (13)$$

Figure 15 shows experimental data along with the deterministic transformation equation that in this case represents the mean trend.

Figure 15: Transformation relationship between SPT N -value and pressure-meter Young's modulus, E

The scatter with respect to the mean trend (deterministic transformation equation), plotted as histogram, is shown in Figure 16.

Figure 16: Histogram of the residual (w.r.t the deterministic transformation equation) Young's modulus, along with fitted probability density function

A zero-mean random variable with Normal distribution and standard deviation of 4041.8 kPa was found to best fit (Figure 16) the scatter with respect to the deterministic equation. The above standard deviation was obtained using maximum likelihood technique.

In this context, one may note that the penetration test is a high strain test (to the order of 10%, refer Figure 65 in) and, the corresponding estimated modulus (Eq. 13) is a high-strain modulus. Hence, to estimate the corresponding low-strain modulus (needed as the input to the von Mises material model, used in this paper), a multiplying factor (low strain correction factor) of 17.25^5 is used. For example, at $N = 15$, a mean high-strain Young's modulus of 10.735 MPa is predicted by Eq. (13). The corresponding mean low-strain Young's modulus used in this paper is $10.735 \text{ MPa} \times 17.25 = 185 \text{ MPa}$. The multiplying factor (low strain correction factor) for standard deviation should, physically, be less than that of the mean. This is because, as the soil is sheared (or, in other words, as soil plastifies), the micro-structure of soil and as a result, our knowledge uncertainty on it increases. This was experimentally observed by . Our probabilistic simulation (refer to) also shows such increase in uncertainty with strain. However, in absence of experimental data for clay, following the probabilistic G/G_{max} versus shear strain curve, suggested by , a multiplying factor (low strain correction factor) of $[1 - (0.2375 - 0.05)/0.05] \times 17.25 = 10.7$ is used for standard deviation. At $N=15$, a standard deviation of 4.04 MPa was estimated using maximum likelihood technique, for high-strain Young's modulus. The corresponding standard deviation of low-strain Young's modulus, then, becomes

⁵assuming $(17.25 - 1)/17.25 = 94 \%$ reduction in modulus at 10% strain, following and presuming that the reduction pattern of Young's modulus follows the same that of shear modulus

$4.04 \times 10.7 = 43.2$ MPa. By assuming undrained condition, one could assume Poisson's ratio to be equal to 0.5 (deterministic) and could transform the Young's modulus to shear modulus as

$$G_{max} = \frac{E_{max}}{2(1 + \nu)} \quad (14)$$

Elastic shear modulus G_{max} would also be a random variable with Normal distribution, as the above equation (Eq. (14)) that relates elastic shear modulus and elastic Young's modulus is a linear equation and hence, the statistical properties of the elastic shear modulus (G_{max}) can easily be obtained using standard techniques. For example, at $N = 15$, the mean and the standard deviation of G_{max} are $185\text{MPa}/(2(1+0.5)) = 61.6$ MPa and $43.2\text{MPa}/(2(1 + 0.5)) = 14.4$ MPa respectively. In this context, it is important to emphasize that the above estimation of the low-strain correction factors would become unnecessary if small-strain shear modulus (G_{max}) is measured directly from geophysical tests or estimated through direct correlation of geophysical test-measured properties (for example shear wave velocity, with SPT N -value). The transformation equations between SPT N -value and shear wave velocity, reported in the literature have not been used in this paper due to lack of reported data points for a meaningful statistical analysis.

In addition to the transformation uncertainty, discussed above, uncertain soil properties will also include significant testing uncertainties. For example, in SPT, the testing uncertainty arises from equipment, procedure and operator errors. proposed typical range of COV for SPT as 15-45%. In this paper, an equivalent of 45% COV is added to undrained shear strength (s_u) and 15% COV is added to elastic shear modulus (G_{max}) to account for SPT testing uncertainties. Larger uncertainty was used for undrained shear strength (s_u) as such strength is not unique but depends on more factors (direction of loading, strain rate, boundary conditions, stress level, and sample disturbance effects, and other factors) than elastic shear modulus G_{max} .

Uncertain spatial variability represents the other important source of uncertainty in soil property. This uncertainty is present because soil properties are measured at few locations then extrapolated/interpolated to all (some) other points of the soil continuum. In other words, in 'estimating' soil properties between two adjacent boreholes, uncertain spatial variability is incurred. This uncertain spatial variability is traditionally accounted for by applying engineering judgment. Probability theory, on the other hand, deals with uncertain spatial variability through random field modeling . Random field modeling characterizes the uncertain spatial variability in terms of standard deviation and correlation length. The standard deviation is added to the uncertainties coming from transformation and testing, while the correlation length can be accounted for, among others, through stochastic elastic-plastic finite element method . In this paper, the uncertain spatial variability has not been explicitly accounted for as the focus of this paper is on point-location (constitutive) behavior. However, one may note that, data of SPT N -value versus undrained shear strength (Figure 14) and SPT N -value versus Young's modulus (Figure 15) contain some spatial variability as SPT is performed at approximately every 30 cm (1 foot) and the blow counts obtained in such way represents average values over that length.

Simulation of G/G_{max} and Damping Behavior Probabilistic elasto–plastic formulation and implementation was used, together with uncertain data sets described in section 3.3, to analyze cyclic behavior of clays. Of particular interest was analysis of material model performance, a simple, elastic–perfectly plastic von Mises, extended into probabilistic space, for a practical problem of undrained cyclic (shear) behavior of clays.

Probabilistic elastic–plastic stress–strain response. Figure 17(a) shows the mean shear stress versus shear strain hysteresis loop for undrained clay modeled using probabilistic von Mises material elastic–perfectly plastic model. Probabilistic elastic–plastic properties (shear modulus G and shear strength s_u) were defined in subsection 3.3 above. Probability distributions for both shear modulus, G and undrained shear strength, s_u were obtained from corresponding SPT N -value of 15. Uncertain clay material was numerically cyclically sheared to $\pm 1.026\%$ shear strain. The cyclic evolution of standard deviation of shear stress is shown in Figure 17(b).

Figure 17: Simulated hysteresis shear stress versus shear strain loop at $\pm 1.026\%$ shear strain: (a) mean and (b) standard deviation behavior

Results shown in Figures 17(a) and (b) were obtained by solving the Fokker–Planck–Kolmogorov equation, with advection and diffusion coefficients numerically, with appropriate initial and boundary conditions. Solution obtained in such a way (in the form of cyclic evolution of probability density function (PDF) of shear stress with shear strain) was then integrated by standard techniques to obtain the evolutionary mean and standard deviation behavior. The details of the solution technique for governing Fokker–Planck–Kolmogorov equation can be found in .

It is important to note that simulation results shown in Figure 17 are obtained using elastic – perfectly plastic von Mises material model and require only two probabilistic soil parameters (their probability distribution) – elastic shear modulus (G_{max}) and undrained shear strength (s_u). If probability distribution of material parameters were neglected and only mean values were used (thus simplifying to deterministic von Mises elastic–perfectly plastic model) simple bi-linear response would results. Such bi-linear response is also shown in Figure 17(a).

Mean response (of the full probability response described by the stress PDF) is non–linear even at very small strain, although, the deterministic model assumes linearity till yielding occurs and then behaves as perfectly plastic material. This is clearly observed from Figure 17(a). Such nonlinear mean response is due to the uncertainty in yield stress, as there is always probability (however small) that elastic–plastic response starts at a very small strain. In addition to that, there also exist a probability that material is elastic at strains past (mean) yielding point, and since the mean solution is an ensemble average of all the possibilities,

such probable elastic influence is extended into plastic range as well. One can visualize this probabilistic yielding effect by observing that within a laboratory specimen (considered generally as a representative volume element, each of large (infinite) number of particle contacts has different and unknown yield strength. Those shear strengths are governed by the PDF of yield strength. At a given strain, some of those particle contacts might be elastic while others might be fully yielding. What is observed in the laboratory experiments is the ensemble average (mean) behavior of all the particle contacts. Similar conclusion was developed by , using probabilistic micro-mechanical simulation. It may be noted that the point-location scale constitutive simulation presented in this paper doesn't account for the scale effect. Such scale effects could be accounted for by quantifying the uncertain spatial variability (for example, through random field modeling) of soil and accounting for it in our simulation. This can be done, for example, through stochastic elastic-plastic finite element method in obtaining local-average constitutive behavior.

Evolution of secant shear modulus. Probabilistic elastic-plastic simulations, described above, were used to obtain evolution of secant shear modulus with shear strain. Figure 18(a) shows mean and mean±standard deviation of the (probabilistic) evolutionary secant shear modulus.

Figure 18: Simulated (a) probabilistic reduction and (b) evolution of coefficient of variation (COV) of secant shear modulus with cyclic shear strain

Compared with the deterministic evolution of secant shear modulus⁶ (also shown in Figure 18(a)), the mean solution predicts a realistic reduction with cyclic shear strain. The region between mean and mean±standard deviation contains the most likely values of evolutionary shear modulus. Coefficient of Variation (COV), which can also be used to visualize uncertainty, is shown in Figure 18(b). The initial COV of secant shear modulus was $[(14.4 \text{ MPa} + 0.15 \times 61.6 \text{ MPa})/61.6 \text{ MPa}] \times 100\% = 38.3\%$. It was calculated from the mean and standard deviation values for G_{max} , obtained earlier, as 61.6 MPa and 14.4 MPa, respectively. The second term in the numerator ($0.15 \times 61.6 \text{ MPa}$) represents the contribution of the testing uncertainty, which was assumed to have a COV of 15% (refer subsection 3.3). It is interesting to observe that COV of secant shear modulus increases with cyclic shear strain. This increase in uncertainty comes from the fact that as the material plastifies, this simple two parameter model becomes less and less accurate. In other words, more detailed investigation of soil structure and more advanced modeling technique need to be used if one wishes to reduce such uncertainty.

The above probabilistic evolution of secant shear modulus (Figure 18) is shown in Figure 19 in a more common form, in terms of variation of G/G_{max} versus shear strain.

⁶Deterministic shear modulus remains constant, equal to $G_{max} = 61.6 \text{ MPa}$ until $\approx 0.3\%$ strain, representing deterministic yield point, before suddenly dropping after yield point.

Figure 19: Simulated probabilistic G/G_{max} behavior

It is important to note that in Figure 19, the normalization of evolutionary mean and mean \pm standard deviation is done by dividing each of those by mean of elastic shear modulus ($\text{Mean}[G_{max}]$). In other words, the upper and lower limits of normalized secant shear modulus, shown in Figure 19 represent $(\text{Mean}[G] \pm \text{Standard Deviation}[G]) / \text{Mean}[G_{max}]$, rather than $G/G_{max} \pm \text{standard deviation}$. The probabilistic evolution of material damping ratio versus shear strain is shown in Figure 20. It is important to note that the upper and lower bounds of damping ratio in Figure 20, were obtained from the hysteresis loops of mean \pm standard deviation of shear stress and shear strain. The mean damping ratio, shown in Figure 20 was obtained from the hysteresis loop of mean shear stress and shear strain.

Figure 20: Simulated probabilistic material damping behavior

In both Figures 19 and 20, the deterministic solutions are also plotted. Though the deterministic solutions fail to predict the realistic soil behavior, probabilistic results, even with the simplest elastic–perfectly plastic model, are comparable to the experimental observations reported in the literature. For example, the probabilistic G/G_{max} and damping ratio results⁷, presented in Figures 19 and 20, compared well with the experimental behavior reported by and for high plasticity clay.

In addition to modulus reduction, the probabilistic approach also captured modulus degradation when the clay material was cyclically sheared repeatedly to a fixed strain level. The hysteresis loops, for clay material sheared repeatedly to $\pm 0.1026\%$ strain, is shown in Figure 21.

Figure 21: Simulated hysteresis shear stress versus shear strain loop, when sheared repeatedly at $\pm 0.1026\%$ strain: (a) mean and (b) standard deviation behavior; First four cycles are shown

Only, first four loops are shown in Figure 21 for clarity. The absolute values of mean and standard deviation of secant shear modulus after each cycle are plotted in Figures 22(a) and (b) respectively.

Figure 22: Simulated probabilistic degradation of shear modulus, when sheared repeatedly at $\pm 0.1026\%$ strain: (a) mean and (b) standard deviation behavior

⁷Their respective mean \pm standard deviation.

The mean shear modulus degraded 8% after 10 cycles at 0.1026% strain. The rate of degradation of mean secant shear modulus was higher initially, but stabilized as the number of cycles increased. The standard deviation of secant shear modulus, on the other hand increased (275% increase after 10 cycles at 0.1026% strain) with number of cycles. It, however, also stabilized after number of cycles increased.

The explanation for increased uncertainty in the secant shear modulus is based on mechanics. With repeated shearing, soil structure is continuously disturbed and hence, our knowledge uncertainty increases. In other words, after repeated shearing, simplistic two-parameter elastic-perfectly plastic model used here cannot model such changes properly. The elastic-plastic probabilistic solution (advection-diffusion equation) aptly captures that fact. The diffusion component, which controls the spread of the response (stress) probability density function, keeps evolving continuously with strain, irrespective of the direction of loading (shearing) until plasticity is fully mobilized with 100% probability, when the diffusion coefficient becomes zero. The advection component, on the other hand, controls the translation of the response (stress) probability density function in the stress-strain domain. This component is a function of loading (shearing) direction, advection coefficient and initial condition at the beginning of each loading direction, which in turn, is a function of the uncertainty present in the system at that state of strain/shearing. The advection component hence gives rise to the degraded modulus after each cycle, until plasticity is fully mobilized with 100% probability. The modulus degradation is, therefore, appearing as a direct consequence of probabilistic yielding of material (clay).

4 Summary

Glossary

Bridge:

Cauchy Stress:

Confining Pressure:

Deterministic:

Dilative:

Dynamic:

Earthquake:

Effective Stress:

Elastic Modulus:

Elasto-Plasticity:

Explicit Algorithm:

Finite Element Method:

Fluid Pressure:

Foundation Piles:

Free Field:

Frequency:

Geomaterial:

Hardware:

Implicit Algorithm:

Liquefaction:

Mass Matrix:

Mud:

Porous Material:

Prediction:

Pressure dependent:

Probabilistic:

Rayleigh Damping:

Sand:

Saturated Soil:

Self-Weight:

Shear Modulus:

Software:

Solid:

Standard Penetration Testing (SPT):

Static:

Stiffness Matrix:

Strain:

Stress:

Structure:

Total Stress:

Validation:

Verification:

Wave Propagation:

Bibliography

Karl Terzaghi. Theoretical Soil Mechanics. Wiley, New York, 1943.

- R. de Boer, R. L. Schiffman, and R. E. Gibson. The origins of the theory of consolidation: The Terzaghi–Fillunger dispute. Géotechnique, 46(2):175–186, 1996.
- Reint de Boer. Highlights in the historical developments of the porous media theory: Toward a consistent macroscopic theory. ASME Applied Mechanics Review, 49(4):201–262, 1996.
- O.C. Zienkiewicz, A.H.C. Chan, M. Pastor, B.A. Schrefler, and T. Shiomi. Computational Geomechanics—with Special Reference to Earthquake Engineering. John Wiley and Sons Ltd., Baffins Lane, Chichester, West Sussex PO19 IUD, England, 1999.
- Patrick J. Roache. Verification and Validation in Computational Science and Engineering. Hermosa Publishers, Albuquerque, New Mexico, 1998. ISBN 0-913478-08-3.
- William L. Oberkampf, Timothy G. Trucano, and Charles Hirsch. Verification, validation and predictive capability in computational engineering and physics. In Proceedings of the Foundations for Verification and Validation on the 21st Century Workshop, pages 1–74, Laurel, Maryland, October 22-23 2002. Johns Hopkins University / Applied Physics Laboratory.
- Jacob Lubliner. Plasticity Theory. Macmillan Publishing Company, New York., 1990.
- Klaus-Jürgen Bathe and L. Wilson, Edward. Numerical Methods in Finite Element Analysis. Prentice Hall Inc., 1976.
- Olgierd Cecil Zienkiewicz and Robert L. Taylor. The Finite Element Method, volume 1. McGraw - Hill Book Company, fourth edition, 1991.
- John Argyris and Hans-Peter Mlejnek. Dynamics of Structures. North Holland in USA Elsevier, 1991.
- Boris Jeremić, Zhao Cheng, Mahdi Taiebat, and Yannis F. Dafalias. Numerical simulation of fully saturated porous materials. International Journal for Numerical and Analytical Methods in Geomechanics, 32(13): 1635–1660, 2008.
- Jean-François Semblat and Alain Pecker. Waves and Vibrations in Soils: Earthquakes, Traffic, Shocks, Construction works. IUSS Press, first edition, 2009. ISBN ISBN-10: 8861980309; ISBN-13: 978-8861980303.
- Thomas J. R. Hughes. The Finite Element Method ; Linear Static and Dynamic Finite Element Analysis. Prentice Hall Inc., 1987.
- Roger G. Ghanem and Pol D. Spanos. Stochastic Finite Elements: A Spectral Approach. Dover Publications, Inc., Mineola, New York, 2003.

- Kallol Sett, Boris Jeremić, and M. Levent Kavvas. Stochastic elastic-plastic finite elements. Computer Methods in Applied Mechanics and Engineering, 200(9-12):997–1007, February 2011. ISSN 0045-7825. doi: DOI:10.1016/j.cma.2010.11.021. URL <http://www.sciencedirect.com/science/article/B6V29-51N7RNC-1/2/7d3ca12b%0a9817a6ddc35f55f7b9df00>.
- B. A. Bilby, L. R. T. Gardner, and A. N. Stroh. Continuous distributions of dislocations and the theory of plasticity. In *IX^e Congrès International de Méchanique Appliquée*, volume VIII, pages 35–44, Université de Bruxelles, 50. Avèue Franklin Roosevelt, 1957.
- Ekkehart Kröner. Allgemeine kontinuumstheorie der versetzungen und eigenspanungen. Archive for Rational Mechanics and Analysis, 4(4):273–334, 1960.
- E. H. Lee and D. T. Liu. Finite-strain elastic-plastic theory with application to plane-wave analysis. Journal of Applied Physics, 38(1):19–27, January 1967.
- N. Fox. On the continuum theories of dislocations and plasticity. Quarterly Journal of Mechanics and Applied Mathematics, XXI(1):67–75, 1968.
- E. H. Lee. Elastic-plastic deformation at finite strains. Journal of Applied Mechanics, 36(1):1–6, 1969.
- J. C. Simo. Algorithms for static and dynamic multiplicative plasticity that preserve the classical return mapping schemes of the infinitesimal theory. Computer Methods in Applied Mechanics and Engineering, 99:61–112, 1992.
- Boris Jeremić, Zhaohui Yang, Zhao Cheng, Guanzhou Jie, Kallol Sett, Mahdi Taiebat, Matthias Preisig, Nima Tafazzoli, Panagiota Tasiopoulou, José Antonio Abell Mena, and Federico Pisanò. Lecture notes on computational geomechanics: Inelastic finite elements for pressure sensitive materials. Technical Report UCD-CompGeoMech-01–2004, University of California, Davis, 1989-2012. available online at: <http://sokocalo.engr.ucdavis.edu/~jeric>.
- Boris Jeremić, Kenneth Runesson, and Stein Sture. A model for elastic-plastic pressure sensitive materials subjected to large deformations. International Journal of Solids and Structures, 36(31/32):4901–4918, 1999.
- W. Karush. Minima of functions of several variables with inequalities as side constraints. Master's thesis, University of Chicago, Chicago, IL., 1939.
- H. W. Kuhn and A. W. Tucker. Nonlinear programming. In Jerzy Neyman, editor, Proceedings of the Second Berkeley Symposium on Mathematical Statistics and Probability, pages 481 – 492. University of California Press, July 31 – August 12 1950 1951.

- Boris Jeremić and Stein Sture. Implicit integrations in elasto–plastic geotechnics. International Journal of Mechanics of Cohesive–Frictional Materials, 2:165–183, 1997.
- Ted Belytschko, Wing Kam Liu, and Brian Moran. Nonlinear finite elements for continua and structures. John Wiley & Sons, 2000.
- Boris Jeremić, Kallol Sett, and M. Levent Kavvas. Probabilistic elasto-plasticity: formulation in 1D. Acta Geotechnica, 2(3):197–210, October 2007.
- Kallol Sett, Boris Jeremić, and M. Levent Kavvas. Probabilistic elasto-plasticity: Solution and verification in 1D. Acta Geotechnica, 2(3):211–220, October 2007a.
- Kallol Sett, Boris Jeremić, and M. Levent Kavvas. The role of nonlinear hardening in probabilistic elasto-plasticity. International Journal for Numerical and Analytical Methods in Geomechanics, 31(7):953–975, June 2007b.
- Boris Jeremić and Kallol Sett. On probabilistic yielding of materials. Communications in Numerical Methods in Engineering, 25(3):291–300, 2009.
- Kallol Sett and Boris Jeremić. Probabilistic yielding and cyclic behavior of geomaterials. International Journal for Numerical and Analytical Methods in Geomechanics, 34(15):1541–1559, 2010. 10.1002/nag.870 (first published online March 11, 2010).
- Kallol Sett and Boris Jeremić. Forward and backward probabilistic simulations in geotechnical engineering. In Magued Iskander, Debra F. Laefer, and Mohamad H. Hussein, editors, Contemporary Topics in Insitu Testing, Analysis, and Reliability of Foundations (Selected Papers from the 2009 International Foundation Congress and Equipment Expo, held in Orlando, FL, from March 15-19, 2009), volume 186 of Geotechnical Special Publications No. 186, pages 1–11. American Society for Civil Engineers, 2009a.
- M. Levent Kavvas. Nonlinear hydrologic processes: Conservation equations for determining their means and probability distributions. Journal of Hydrologic Engineering, 8(2):44–53, March 2003.
- Kari Karhunen. Über lineare methoden in der wahrscheinlichkeitsrechnung. Ann. Acad. Sci. Fennicae. Ser. A. I. Math.-Phys., 37:1–79, 1947.
- M. Loève. Fonctions aleatoires du second ordre. Supplement to P. Levy, Processus Stochastic et Mouvement Brownien, Gauthier-Villars, Paris, 1948.
- N. Wiener. The homogeneous chaos. American Journal of Mathematics, 60:897–936, 1938.

- William Oberkampf. Material from the short course on verification and validation in computational mechanics. Albuquerque, New Mexico, July 2003.
- Todd Veldhuizen. Software libraries and their reuse: Entropy, kolmogorov complexity, and zipf's law. In David Musser, editor, Library-Centric Software Design LCSD'05. Object-Oriented Programming, Systems, Languages and Applications, October 2005.
- Joshua Bloch. How to design a good api and why it matters. In David Musser, editor, Library-Centric Software Design LCSD'05. Object-Oriented Programming, Systems, Languages and Applications, October 2005. Presentation Slides.
- Boris Jeremić and Guanzhou Jie. Plastic domain decomposition method for parallel elastic-plastic finite element computations in geomechanics. Technical Report UCD-CompGeoMech-03-07, University of California, Davis, 2007. available online: <http://sokocalo.engr.ucdavis.edu/~jeremic/wwwpublications/CV-R24.pdf>.
- Boris Jeremić and Guanzhou Jie. Parallel soil-foundation-structure computations. In N.D. Lagaros M. Papdrakakis, D.C. Charnpis and Y. Tsompanakis, editors, Progress in Computational Dynamics and Earthquake Engineering. Taylor and Francis Publishers, 2008.
- Francis Thomas McKenna. Object Oriented Finite Element Programming: Framework for Analysis, Algorithms and Parallel Computing. PhD thesis, University of California, Berkeley, 1997.
- Boris Jeremić and Zhaohui Yang. Template elastic-plastic computations in geomechanics. International Journal for Numerical and Analytical Methods in Geomechanics, 26(14):1407-1427, 2002.
- Boris Jeremić and Stein Sture. Tensor data objects in finite element programming. International Journal for Numerical Methods in Engineering, 41:113-126, 1998.
- Satish Balay, Kris Buschelman, William D. Gropp, Dinesh Kaushik, Matthew G. Knepley, Lois Curfman McInnes, Barry F. Smith, and Hong Zhang. PETSc Web page, 2001. <http://www.mcs.anl.gov/petsc>.
- Satish Balay, Kris Buschelman, Victor Eijkhout, William D. Gropp, Dinesh Kaushik, Matthew G. Knepley, Lois Curfman McInnes, Barry F. Smith, and Hong Zhang. PETSc users manual. Technical Report ANL-95/11 - Revision 2.1.5, Argonne National Laboratory, 2004.
- Satish Balay, William D. Gropp, Lois Curfman McInnes, and Barry F. Smith. Efficient management of parallelism in object oriented numerical software libraries. In E. Arge, A. M. Bruaset, and H. P. Langtangen, editors, Modern Software Tools in Scientific Computing, pages 163-202. Birkhäuser Press, 1997.

- Timothy A. Davis and Iain S. Duff. A combined unifrontal/multifrontal method for unsymmetric sparse matrices. Technical Report TR97-016 (UofF) and TR-97-046 (RAL), University of Florida and Rutherford Appleton Laboratory, 1997a.
- Timothy A. Davis and Iain S. Duff. An unsymmetric-pattern multifrontal method for sparse LU factorization. SIAM Journal of Matrix Analysis and Applications, 18(1):140–158, 1997b.
- T.A. Davis and I.S. Duff. A combined unifrontal/multifrontal method for unsymmetric sparse matrices. ACM Transactions on Mathematical Software, 25(1):1–19, 1999. URL <http://doi.acm.org/10.1145/305658.287640>.
- T.A. Davis. A column pre-ordering strategy for the unsymmetric-pattern multifrontal method. ACM Transactions on Mathematical Software, 30(2):165–195, 2004a. URL <http://doi.acm.org/10.1145/992200.992205>.
- T.A. Davis. Algorithm 832: Umfpack, an unsymmetric-pattern multifrontal method. ACM Transactions on Mathematical Software, 30(2):196–199, 2004b. URL <http://doi.acm.org/10.1145/992200.992206>.
- George Karypis, Kirk Schloegel, and Vipin Kumar. ParMETIS: Parallel Graph Partitioning and Sparse Matrix Ordering Library. University of Minnesota, 1998.
- B. Jeremić, N. Tafazzoli, B. Kamrani, Y.C. Chao, C.G. Jeong, P. Tasiopoulou, K. Sett, A. Kammerer, N. Orbović, and A. Blahoianu. On seismic soil structure interaction simulations for nuclear power plants. In Proceedings of the OECD – NEA – IAGE – ISSC Workshop on Soil Structure Interaction Knowledge and Effect on the Seismic Assessment of NPPs Structures and Components, 2010.
- B. Jeremić, A. Kammerer, N. Tafazzoli, and B. Kamrani. The NRC ESSI Simulator. In B.K.Dutta, editor, Proceedings of the 21st SMiRT (Structural Mechanics in Reactor Technology) Conference, 2011. Paper # 550.
- Boris Jeremić, Guanzhou Jie, Matthias Preisig, and Nima Tafazzoli. Time domain simulation of soil–foundation–structure interaction in non–uniform soils. Earthquake Engineering and Structural Dynamics, 38(5):699–718, 2009.
- Gregory Fenves and Mathew Dryden. Nees sfsi demonstration project. NEES project meeting, TX, Austin, August 2005.
- M. Dryden. Validation of simulations of a two–span reinforced concrete bridge. Submitted in partial satisfaction of requirements for a Ph.D. degree at the University of California at Berkeley, 2006.

- E. Spacone, F.C. Filippou, and F.F. Taucer. Fibre beam–column model for non–linear analysis of r/c frames 1. formulation. Earthquake Engineering and Structural Dynamics, 25:711–725, 1996.
- Jacobo Bielak, Kostas Loukakis, Yoshiaki Hisada, and Chaiki Yoshimura. Domain reduction method for three–dimensional earthquake modeling in localized regions. part I: Theory. Bulletin of the Seismological Society of America, 93(2):817–824, 2003.
- Chaiki Yoshimura, Jacobo Bielak, and Yoshiaki Hisada. Domain reduction method for three–dimensional earthquake modeling in localized regions. part II: Verification and examples. Bulletin of the Seismological Society of America, 93(2):825–840, 2003.
- Kandiah Arulanandan and Ronald F. Scott, editors. Verification of Numerical Procedures for the Analysis of Soil Liquefaction Problems. A. A. Balkema, 1993.
- Kok-Kwang Phoon and Fred H. Kulhawy. Evaluation of geotechnical property variability. Canadian Geotechnical Journal, 36:625–639, 1999a.
- A. Hara, T. Ohta, M. Niwa, S. Tanaka, and T. Banno. Shear modulus and shear strength of cohesive soils. Soils and Foundations, 14(3):1–12, 1974.
- S. Ohya, T. Imai, and M. Matsubara. Relationship between N-value by SPT and LLT pressuremeter results. In Proceedings of the 2nd. European Symposium on Penetration Testing, volume 1, pages 125–130, Amsterdam, 1982.
- Federal Highway Administration. Geotechnical engineering circular No 5. U.S. Department of Transportation, Publication No. FHWA-IF-02-034, April 2002.
- I. M. Idriss. Response of soft soil sites during earthquakes. In Proceedings of the Symposium to Honor Professor H. B. Seed, pages 273–289. BiTech Publishers, Vancouver, B.C., Canada, 1990.
- K. H. Stokoe II, R. B. Darendeli, R. B. Gilbert, F.-Y. Menq, and W. K. Choi. Development of a new family of normalized modulus reduction and material damping curves. In International Workshop on Uncertainties in Nonlinear Soil Properties and their Impact on Modeling Dynamic Soil Response, PEER Headquarters, UC Berkeley, March 18-19, 2004, Plenary Paper, http://peer.berkeley.edu/lifelines/Workshop304/pdf/Stokoe_PlenaryPaper.pdf, 2004a. PEER.
- Kallol Sett and Boris Jeremić. Probabilistic yielding and cyclic behavior of geomaterials. International Journal for Numerical and Analytical Methods in Geomechanics, 2009b. in print.

- Nilsun Hasancebi and Resat Ulusay. Empirical correlations between shear wave velocity and penetration resistance for ground shaking assessments. Bulletin of Engineering Geology and Environment, 66(2): 203–213, May 2007.
- M. K. Jafari, A. Shafiee, and A. Ramzkhah. Dynamic properties of fine grained soils in south of Tehran. Iranian Journal of Seismology and Earthquake Engineering, 4(1):25–35, 2002.
- K. Pitilakis, D. Raptakis, K. Lontzetidis, T. Tika-Vasilikou, and D. Jongmans. Geotechnical and geophysical description of Euro-seistests, using field and laboratory tests, and moderate strong ground motions. Journal of Earthquake Engineering, 3(3):381–409, 1999.
- T. Imai. P- and S-wave velocities of the ground in Japan. In Proceedings of the IX International Conference on Soil Mechanics and Foundation Engineering, pages 127–132, Tokyo, Japan, 1977. Volume 2.
- Kok-Kwang Phoon and Fred H. Kulhawy. Characterization of geotechnical variability. Canadian Geotechnical Journal, 36:612–624, 1999b.
- Charles C. Ladd. Stability evaluation during staged construction. Journal of Geotechnical Engineering, 117 (4):540–615, April 1991.
- Paul W. Mayne. Cone penetration testing state-of-practice. Final Report NCHRP Project 20-05; Task 37-14, Georgia Institute of Technology, Atlanta, GA, February 2007. Transportation Research Board Synthesis Study.
- Don J. DeGroot and Gregory B. Baecher. Estimating autocovariance of in-situ soil properties. Journal of Geotechnical Engineering, 119(1):147–166, January 1993.
- Gordon A. Fenton. Estimation of stochastic soil models. Journal of Geotechnical and Geoenvironmental Engineering, 125(6):470–485, June 1999a.
- Gordon A. Fenton. Random field modeling of CPT data. Journal of Geotechnical and Geoenvironmental Engineering, 125(6):486–498, June 1999b.
- Z. Hashin. Analysis of composite materials. Journal of Applied Mechanics, 50:481–505, 1983.
- Itai Einav and Ian F. Collins. A thermomechanical framework of plasticity based on probabilistic micromechanics. Journal of Mechanics of Materials and Structures, 3(5):867–892, May 2008.
- Mladen Vucetic and Ricardo Dobry. Effect of soil plasticity on cyclic response. Journal of Geotechnical Engineering, 117(1):89–107, January 1991.

K. H. Stokoe II, M. B. Darendeli, R. B. Gilbert, F. Y. Menq, and W. K. Choi. Development of a new family of normalized modulus reduction and material damping curves. In Proceedings of International Workshop on Uncertainties in Nonlinear Soil Properties and their Impact on Modeling Dynamic Soil Response, PEER Headquarters, UC Berkeley, March 18-19, 2004, Opinion Paper. PEER, 2004b.

Biographical Sketches

Boris Jeremić is a Professor at the Department of Civil and Environmental Engineering at the University of California, Davis, California and is a Faculty Scientist in the Earth Science Division of the Lawrence Berkeley National Laboratory, Berkeley, California. He earned his Civil Engineering Diploma Degree from the University of Belgrade, Yugoslavia (1989), Master of Engineering (1994) and Doctor of Philosophy (1997) in Civil Engineering from the University of Colorado at Boulder, Colorado. From 1989 to 1992 he worked as staff engineer for Energoprojekt Engineering Corporation in Belgrade, Yugoslavia and at the Bekhme Dam Site in Iraq. Professor Jeremić's interests are related to high fidelity modeling and simulation of inelastic solids and structures. Current work is on development and use of computational libraries/systems for simulation of static and dynamic, deterministic and probabilistic, inelastic behavior of engineering solids and structures. Focus is on the development and use of methods that reduce Kolmogorov complexity and modeling uncertainty. Research and teaching is geared toward development of tools (programs, educational material) for research and practice.

Kallol Sett is an Assistant Professor in the Department of Civil Engineering at the University of Akron, Ohio. He earned his bachelors degree with honors from Jadavpur University, Calcutta, India in 1997, his masters degree from the University of Houston in 2003, and his doctorate from the University of California, Davis in 2007, all in civil engineering. He has taught civil engineering courses at the University of California, Davis and has worked for the California Department of Transportation as well as Afcons Infrastructure Limited in Bombay, India. His research interests are in assessment and mitigation of risks in civil engineering infrastructure systems, with emphasis on geotechnical systems, whereas his teaching interests lie in deterministic and stochastic solid mechanics, with emphasis in geomechanics, and application of probability theory in civil engineering.

Mahdi Taiebat is an Assistant Professor of Civil Engineering at the University of British Columbia. He received his B.Sc. and M.Sc. degrees in Civil Engineering from Sharif University of Technology in 2001 and 2003 and his Ph.D. in Civil Engineering from the University of California, Davis in 2008. After receiving his Ph.D., he was awarded a post-doctoral fellowship to work in the computational geomechanics division of

the Norwegian Geotechnical Institute. He has received the UC Davis excellence in geotechnical engineering award in 2007 and the ASCE Norman Medal in 2012. At UBC he is responsible for teaching courses in Soil Mechanics, Advanced Soil Mechanics, and Geotechnical Earthquake Engineering. His research interests include development and implementation of advanced constitutive models for engineering materials and their applications in geotechnical earthquake engineering and soil-structure-interaction problems.

Nima Tafazzoli is a Post-Doctoral Researcher in the department of Civil and Environmental Engineering at the University of California, Davis. He received his B.Sc. degree in 2004 from University of Tehran and his M.Sc. in 2006 engineering from Iran University of Science and Technology. He then joined University of California, Davis and obtained his Ph.D. in 2012. He also has taught several courses at University of California, Davis. His research interests include computational mechanics, modeling and simulation of soil-structure systems, and geotechnical earthquake engineering.

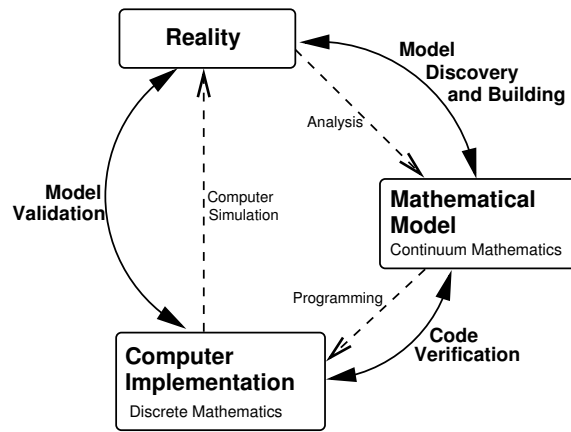


Figure 1: Schematic representation of role of verification and validation in relation to real model

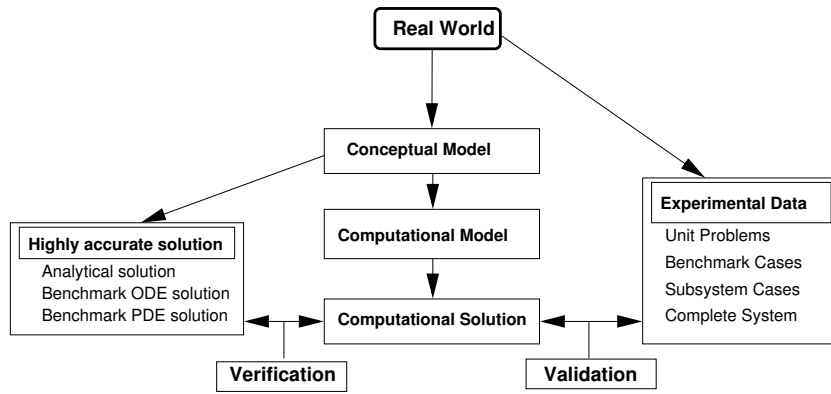


Figure 2: Schematic representation of relationship between verification and validation

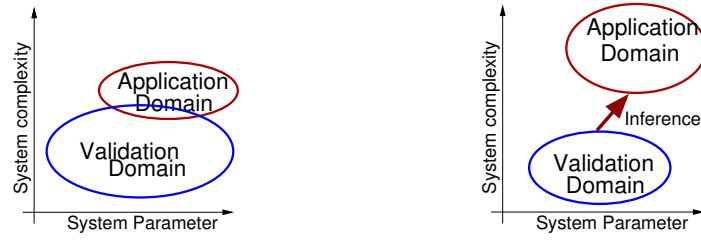


Figure 3: Schematic representation of partial or no overlap of verification and application domains

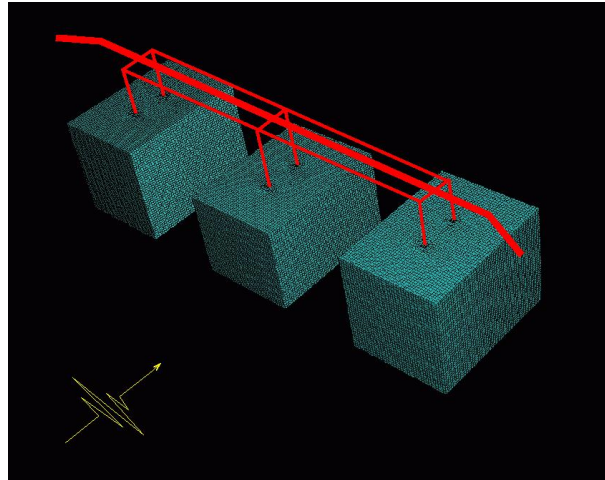


Figure 4: Detailed Three Bent Prototype SFSI Finite Element Model, 484,104 DOFs, 151,264 Elements used for most simulation in this study

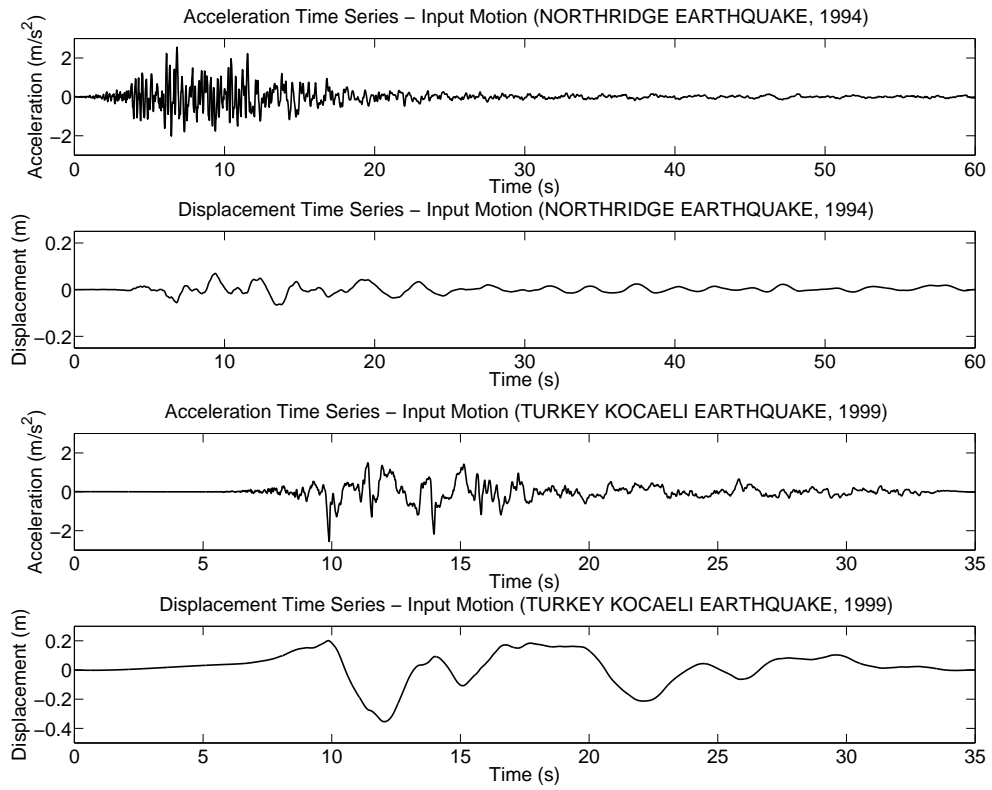


Figure 5: Input motions: short period (Northridge) and long period (Kocaeli)

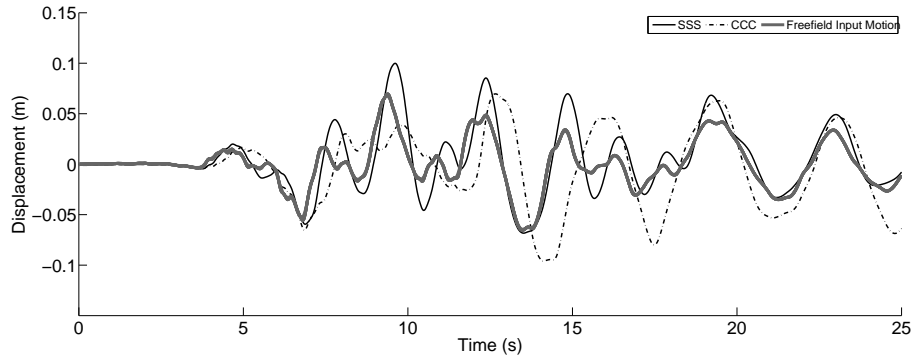


Figure 6: Comparison of free field versus measured (prototype model) motions at the base of left bent for the short period motions (Northridge) for all clay (CCC) and all sand (SSS) soils

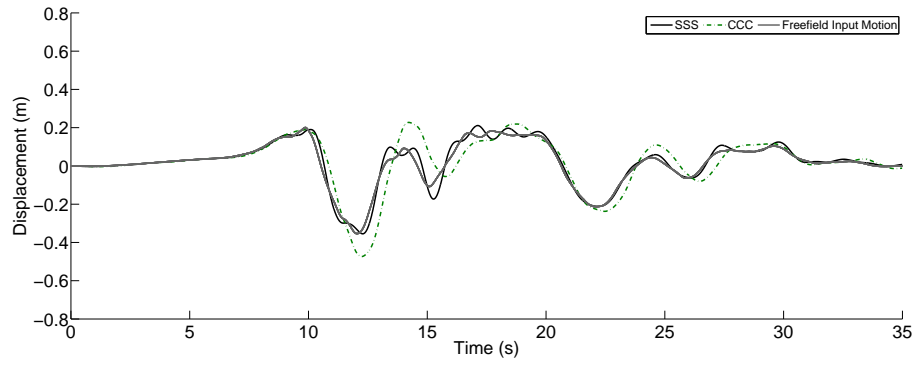


Figure 7: Comparison of free field versus measured (prototype model) motions at the base of left bent for the long period motions (Kocaeli) for all clay (CCC) and all sand (SSS) soils

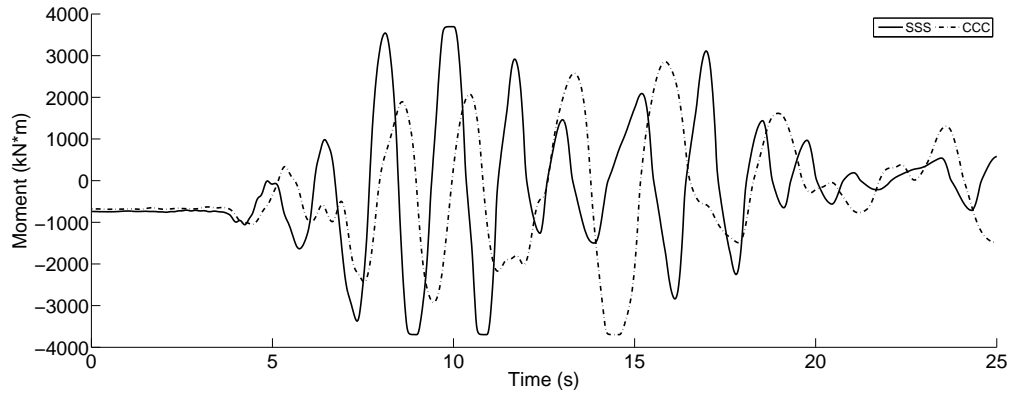


Figure 8: Simulated bending moment time series (top of left pier) for short period motion (Northridge), for all clay (CCC) and all sand (SSS) soils

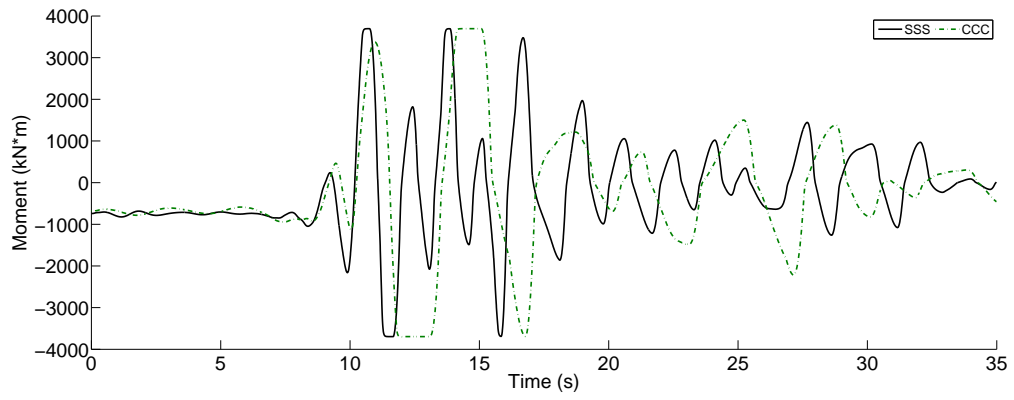


Figure 9: Simulated bending moment time series (top of left pier) for long period motion (Kocaeli), for all clay (CCC) and all sand (SSS) soils

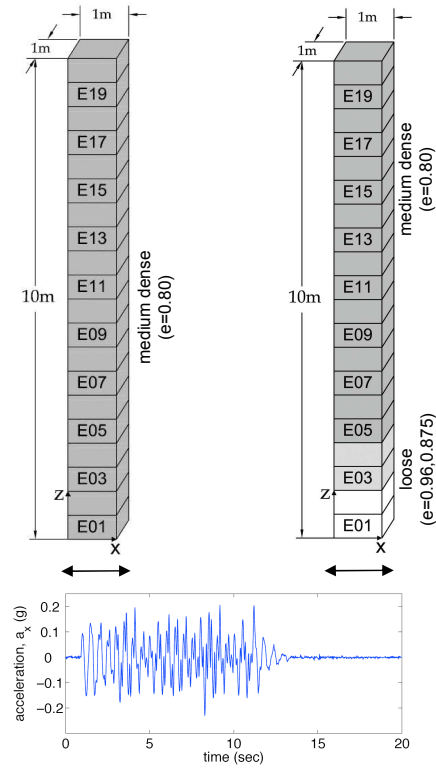


Figure 10: Illustration of the problem in terms of the soil layering, the finite element mesh, and the input base acceleration

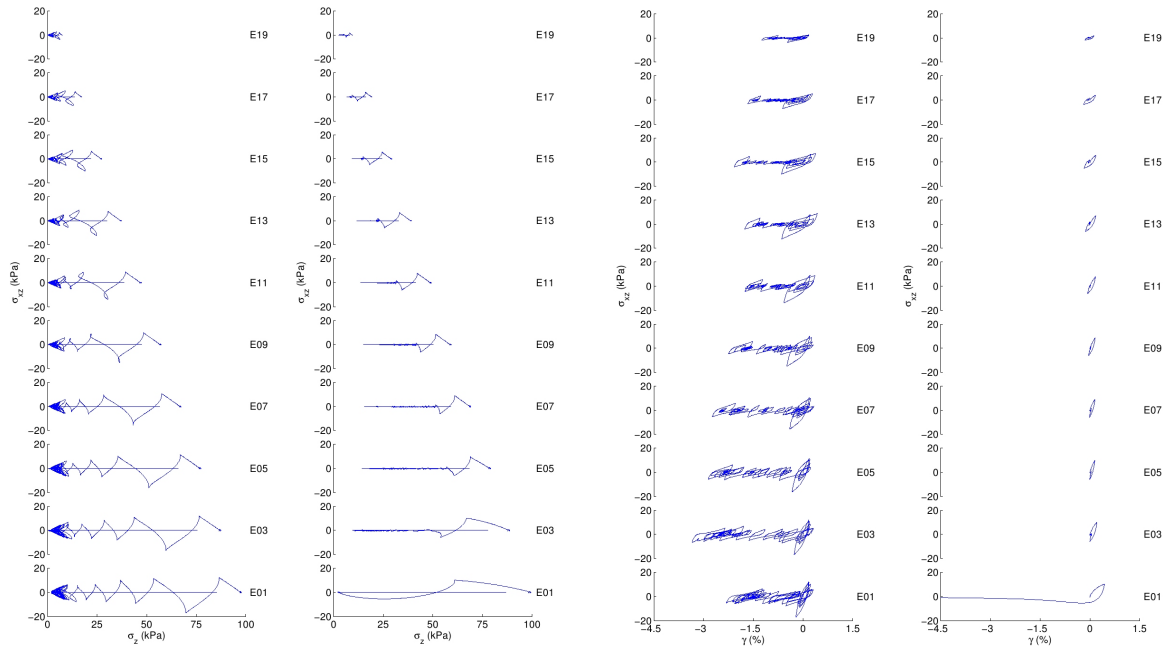


Figure 11: (left) Variation of shear stress σ_{xz} vs vertical effective stress σ_z for Elements E01 – E19 during and after shaking; (right) Variation of shear stress σ_{xz} vs shear strain γ for Elements E01 – E19 during and after shaking

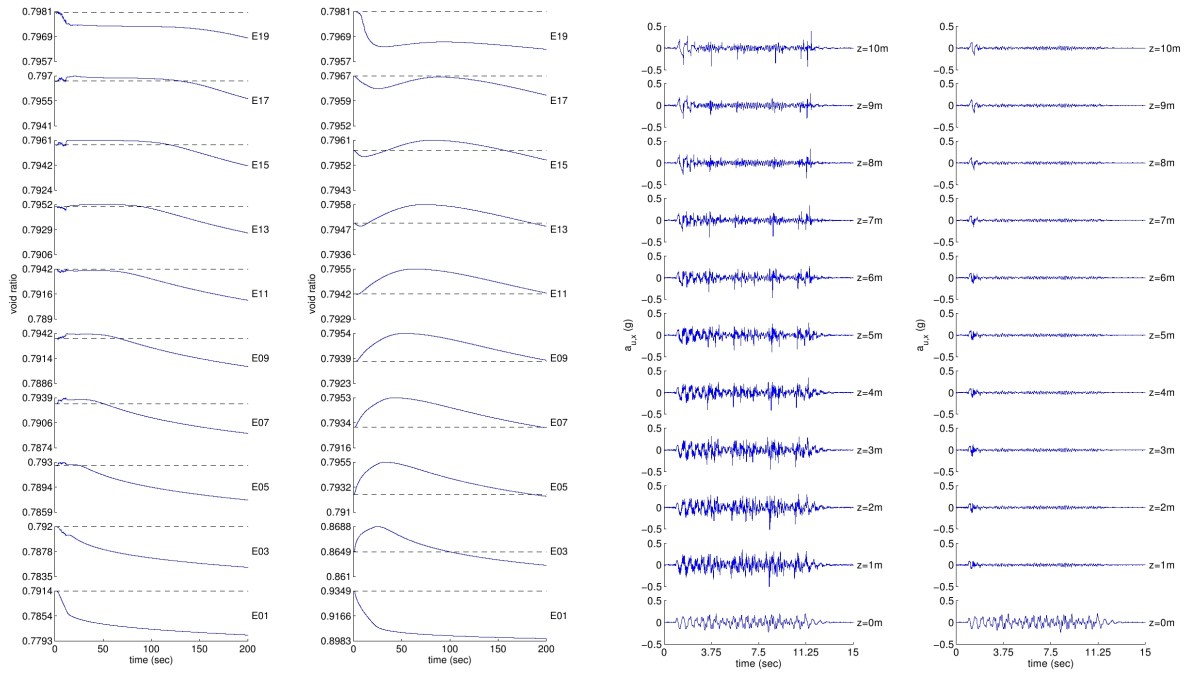


Figure 12: (left) Variation with time of void ratio e for Elements E01 – E19 during and after shaking ; (right) Time history of horizontal component of acceleration in solid part of the mixture $a_{u,x}$ for nodes at different elevations during shaking

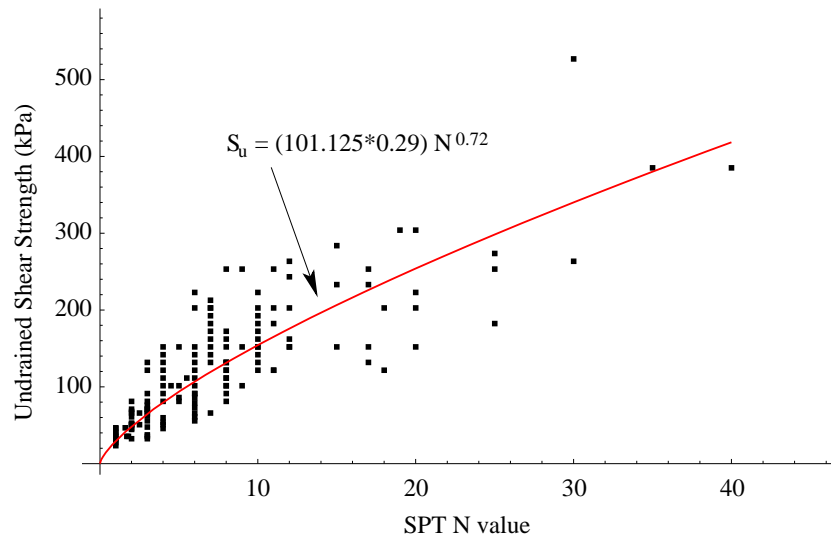


Figure 13: Transformation relationship between SPT N -value and undrained shear strength, s_u

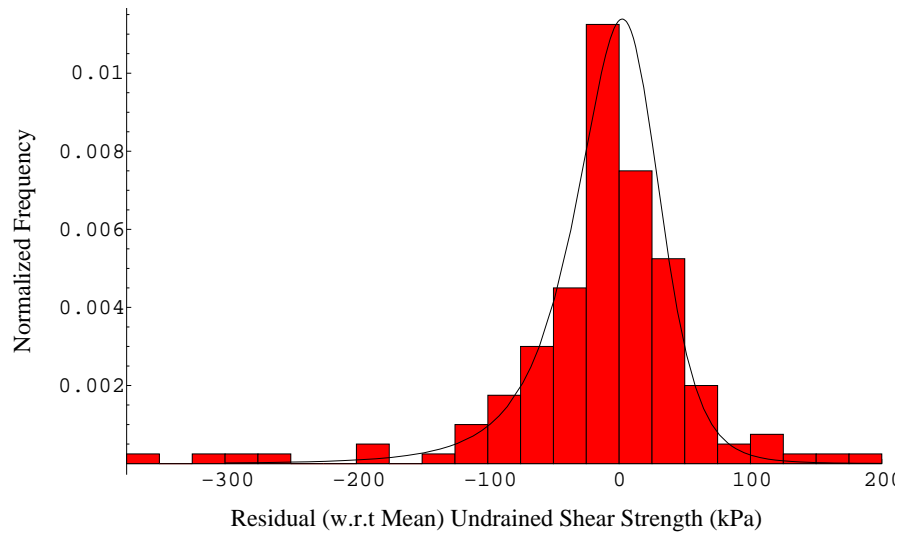


Figure 14: Histogram of the residual (w.r.t the deterministic transformation equation) undrained strength, along with fitted probability density function

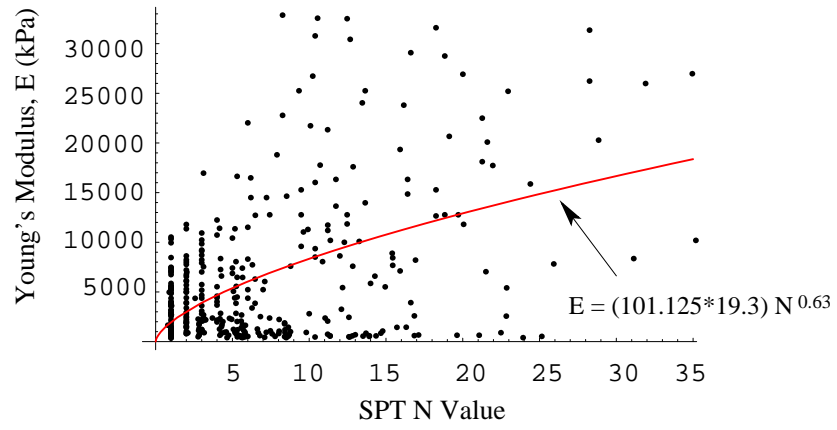


Figure 15: Transformation relationship between SPT N -value and pressure-meter Young's modulus, E

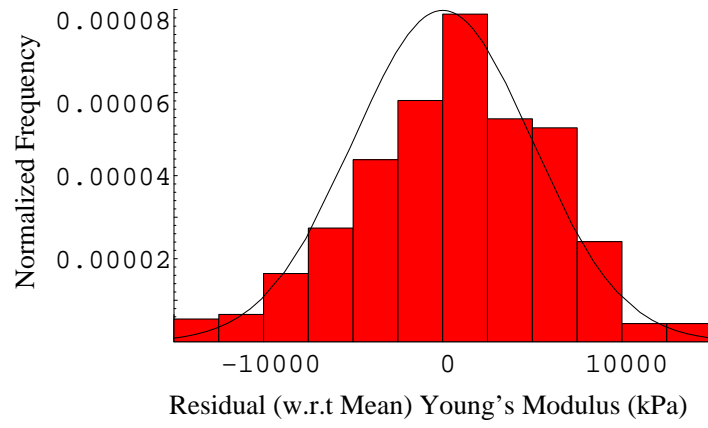


Figure 16: Histogram of the residual (w.r.t the deterministic transformation equation) Young's modulus, along with fitted probability density function

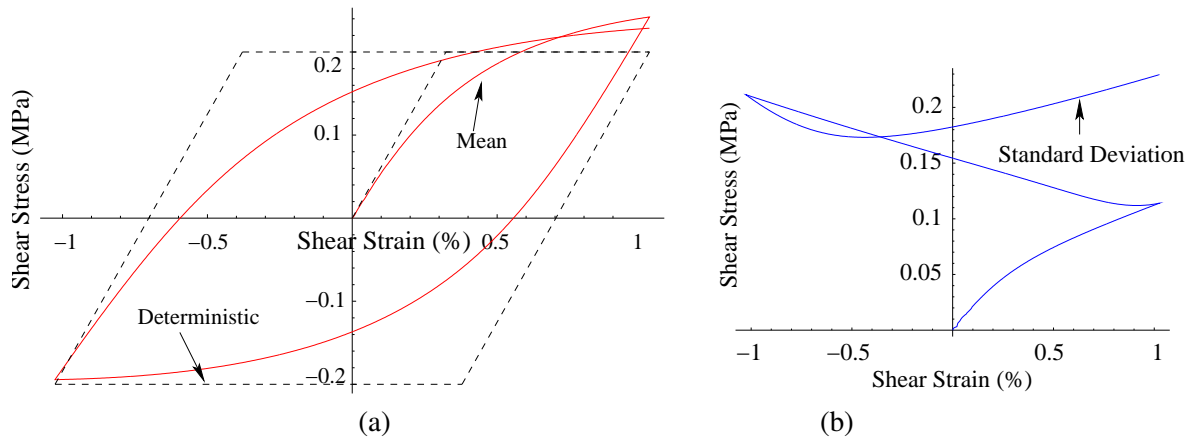


Figure 17: Simulated hysteresis shear stress versus shear strain loop at $\pm 1.026\%$ shear strain: (a) mean and (b) standard deviation behavior

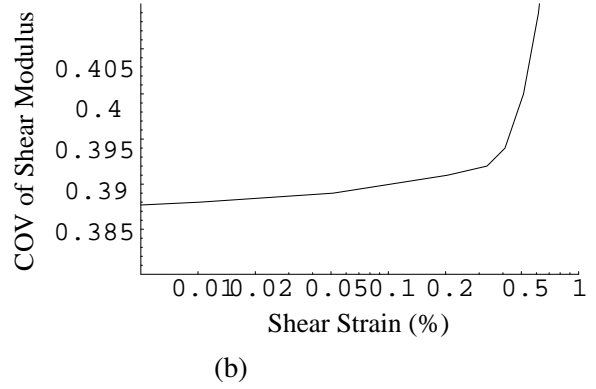
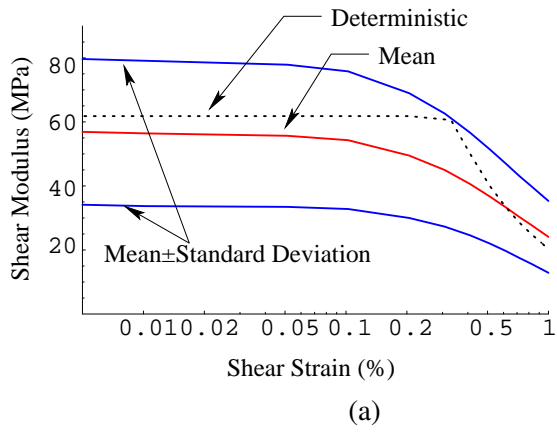


Figure 18: Simulated (a) probabilistic reduction and (b) evolution of coefficient of variation (COV) of secant shear modulus with cyclic shear strain

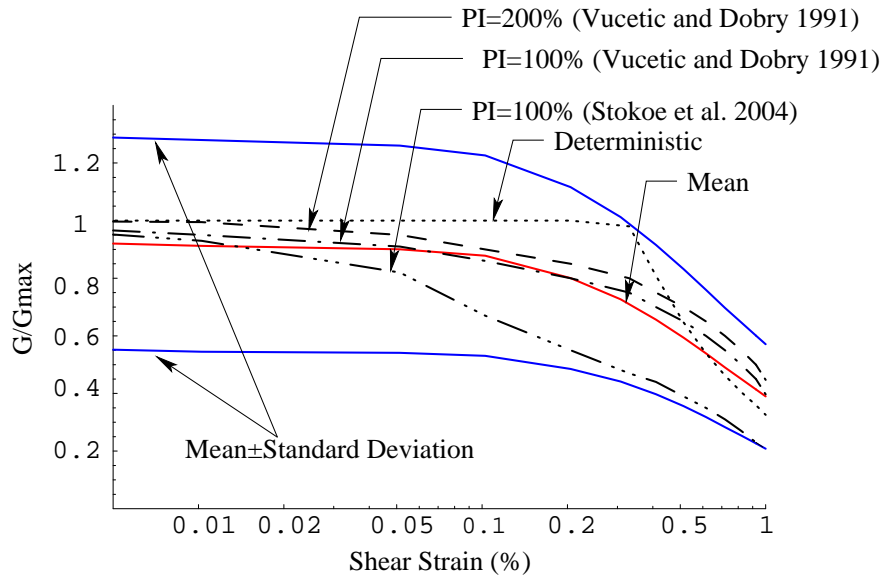


Figure 19: Simulated probabilistic G/G_{max} behavior

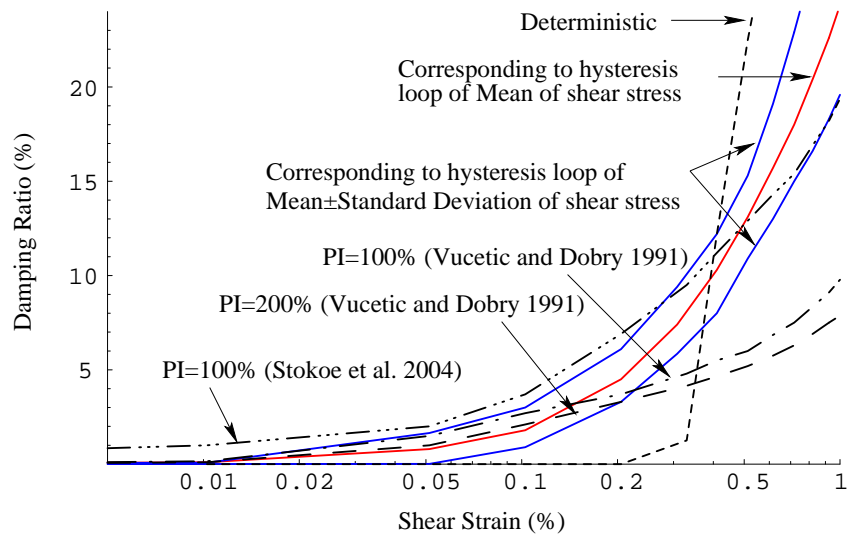


Figure 20: Simulated probabilistic material damping behavior

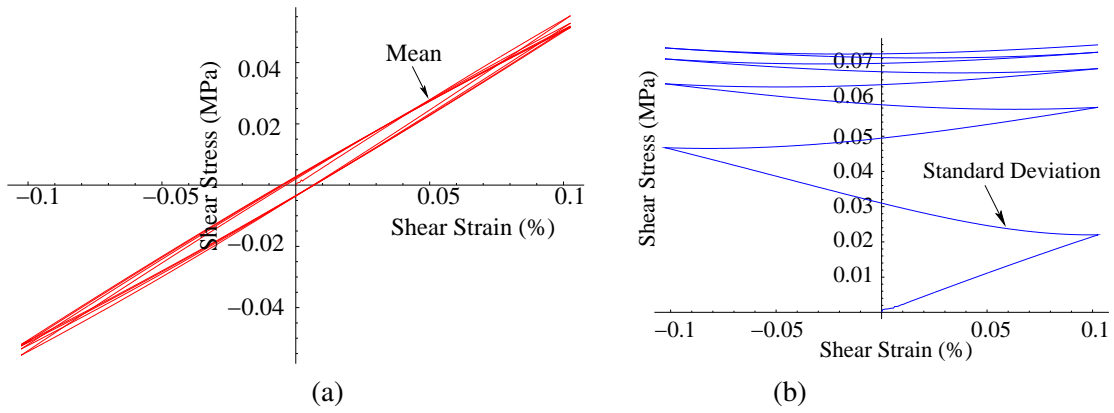
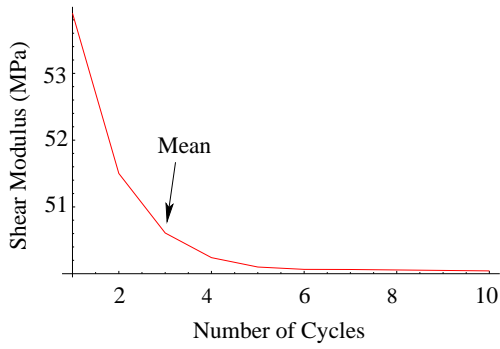
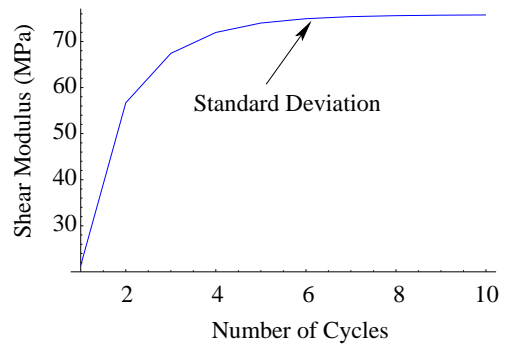


Figure 21: Simulated hysteresis shear stress versus shear strain loop, when sheared repeatedly at $\pm 0.1026\%$ strain: (a) mean and (b) standard deviation behavior; First four cycles are shown



(a)



(b)

Figure 22: Simulated probabilistic degradation of shear modulus, when sheared repeatedly at $\pm 0.1026\%$ strain: (a) mean and (b) standard deviation behavior